Heterogeneous diffusion processes and nonergodicity with Gaussian colored noise in layered diffusivity landscapes

Yong Xu,[1,2,*] Xuemei Liu,[1] Yongge Li,[1,3,†] and Ralf Metzler[4,‡]

[1]*School of Mathematics and Statistics, Northwestern Polytechnical University, Xi'an 710072, China*
[2]*MIIT Key Laboratory of Dynamics and Control of Complex Systems, Northwestern Polytechnical University, Xi'an 710072, China*
[3]*Center for Mathematical Sciences, Huazhong University of Science and Technology, Wuhan 430074, China*
[4]*Institute for Physics and Astronomy, University of Potsdam, 14476 Potsdam-Golm, Germany*

(Received 9 November 2019; accepted 22 October 2020; published 2 December 2020)

Heterogeneous diffusion processes (HDPs) with space-dependent diffusion coefficients $D(x)$ are found in a number of real-world systems, such as for diffusion of macromolecules or submicron tracers in biological cells. Here, we examine HDPs in quenched-disorder systems with Gaussian colored noise (GCN) characterized by a diffusion coefficient with a power-law dependence on the particle position and with a spatially random scaling exponent. Typically, $D(x)$ is considered to be centerd at the origin and the entire x axis is characterized by a single scaling exponent α. In this work we consider a spatially random scenario: in periodic intervals ("layers") in space $D(x)$ is centerd to the midpoint of each interval. In each interval the scaling exponent α is randomly chosen from a Gaussian distribution. The effects of the variation of the scaling exponents, the periodicity of the domains ("layer thickness") of the diffusion coefficient in this stratified system, and the correlation time of the GCN are analyzed numerically in detail. We discuss the regimes of superdiffusion, subdiffusion, and normal diffusion realisable in this system. We observe and quantify the domains where nonergodic and non-Gaussian behaviors emerge in this system. Our results provide new insights into the understanding of weak ergodicity breaking for HDPs driven by colored noise, with potential applications in quenched layered systems, typical model systems for diffusion in biological cells and tissues, as well as for diffusion in geophysical systems.

DOI: 10.1103/PhysRevE.102.062106

I. INTRODUCTION

Anomalous diffusion processes [1–11] are abundant in the dynamics of nanoparticles [12–14], in plasma [15] and spin glasses [16,17], in the cytoplasm of living cells [11,18–27], in groundwater transport [28–30], for atmospheric meteorological changes [31], etc. These systems follow the power-law time dependence for the mean-squared displacement (MSD),

$$\langle x^2(t)\rangle \simeq t^{\beta}, \tag{1}$$

where β is the anomalous scaling exponent [1,6,7,32]. For $\beta = 1$ normal diffusion is realized, while for $\beta < 1$, $1 < \beta < 2$, $\beta = 2$, and $\beta > 2$ the process is called subdiffusive, superdiffusive, ballistic, and hyperdiffusive, respectively [1,33,34]. The case $\beta = 0$ is the limit of complete particle localisation [35]. To obtain an MSD of the form Eq. (1), a number of mathematical models have been proposed, including the description by fractional Brownian motion, fractional Langevin equation, Lévy walks, continuous time random walks, etc [1,5–7,9]. Although most of these models describe spatially homogeneous scenarios, the diffusivity may be an explicit local function of the tracer's position, $D(x)$. For diffusion of pollutants in underground aquifers, for instance, spatial variations in the transport characteristics of $D(x)$ are due to soil stratification [35,36]. For eukaryotic [21] and prokaryotic cells [37] the local diffusivity of endogeneous and artificially introduced tracers also shows significant variations from one location to another. Moreover, when the tracer's size is comparable to the periodicity of the local compartmentalized structure in cells, the motion of the tracer can also be hindered by cage effects [38,39]. Such heterogeneous and stratified systems require that a position-dependent diffusivity is included in the description giving rise to the so-called heterogeneous diffusion processes (HDPs) [40–44].

Recently, anomalous diffusion in conjunction with disordered environments and ergodic properties of these systems have attracted considerable attentions [45–53]. For example, the effects of ergodicity (see below), symmetry breaking, and velocity relaxation for anomalous diffusion in periodic systems have been considered [45]. Ergodicity breaking and aging for Brownian dynamics (without damping) with quenched disorder were also investigated [46]. These two models belong to the class of generalized grey Brownian motion. Nonergodicity, fluctuations, and criticality of HDPs were studied in detail in Refs. [40,41,47]. The random-diffusivity approach on the level of stochastic differential equations has been considered and two models of Brownian yet non-Gaussian diffusion were recently proposed [48]. Moreover, anomalous diffusion was investigated in random dynamical systems, see Ref. [49].

The presence of quenched disorder often prevents a system from reaching thermodynamic equilibrium [54]. For instance, the behavior of ferromagnetic quantum transits [55],

*hsux3@nwpu.edu.cn
†liyonge@nwpu.edu.cn
‡rmetzler@uni-potsdam.de

orientational glasses [56], and creep rupture of composites [57] possess quenched-disorder characteristics. In amorphous semiconductors, quenched traps affect anomalous diffusion and ageing [58–61]. Quenched disorder is revealed for noninteracting particles on lattices and for crystal-growth processes [62]. Therefore, the studies of diffusion in quenched disordered environments are called for. The effects of various types of noise, such as Lévy noise [63–66], Poisson noise [67], fractional Gaussian noise [68], and Gaussian noise [69] on stochastic systems have been extensively studied. Diffusion under nonstandard noise excitations is of interest in its own right. There exist numerous studies on anomalous diffusion with different kinds of noise sources. The influence of Gaussian white noise (GWN) on particle trajectories in some disordered systems [70] and the phenomenon of ergodicity breaking for HDPs were studied [40,41,47]. Subdiffusion within a single protein molecules was examined [71–74], in particular with fractional Gaussian noise (see also Refs. [75,76] for the ergodic properties of fractional Brownian motion). Furthermore, the exact results for the nonergodicity of d-dimensional generalized Lévy walks [77] and neuronal messenger ribonucleoprotein transport following aging Lévy-type walks [78] were recently explored.

In practical applications, there are several types of colored noise such as pink, blue, grey, etc. [79]. From the noise perspective, Gaussian colored noise (GCN) is widely studied in stochastic dynamical systems, for instance, for stationary distributions of rare events [80], the wing model [81], in nonlinear vibration energy-harvesting system [82], for transport in a confined ratchet [83], etc. However, the influence of colored noise on the properties of HDPs has not been reported so far, to the best of our knowledge. The main objective of the current study is to examine the dynamics and nonergodicity of HDPs with position-dependent diffusivity in layered quenched systems agitated by exponentially correlated GCN source.

The paper is organized as follows. In Sec. II HDPs driven by GCN are introduced. In Sec. III we provide the mathematical definitions of the main physical observables we study. In that section, we also analyze the effects of the model parameters on particle diffusion in terms of the MSD and the time-averaged MSD (TAMSD), including the correlation time of GCN, the domain periodicity of the system, and the variance of the diffusivity exponent. In Sec. IV the ergodicity breaking and non-Gaussianity parameters are investigated for different diffusion scenarios. Finally, our conclusions are summarized in Sec. V.

II. MODEL DESCRIPTION AND MAIN EQUATIONS

We consider one-dimensional HDPs driven by GCN and with a position-dependent random diffusivity. The governing Langevin equation for the particle position $x(t)$ at time t is [84–87]

$$\frac{dx(t)}{dt} = \sqrt{2D(x)}\xi(t), \tag{2}$$

where the diffusion coefficient has the form

$$D(x) = D_0(|x|^\alpha + D_{\rm off}). \tag{3}$$

We fix below $D_0 = 0.01$ and $D_{\rm off} = 0.001$. $D_{\rm off}$ is a small constant added to avoid a singularity of $D(x)$ at $x = 0$ [40,47]. Generally, for a given, fixed exponent $\alpha < 0$ in the $D(x)$ function yields subdiffusion, $\alpha = 0$ is the limit of normal diffusion, and $\alpha > 0$ corresponds to superdiffusion [40,41,47]. However, in some physical systems, such as for tracer diffusion in the cell cytoplasm or in groundwater transport, due to the existence of layers with varying diffusivity, $D(x)$ may change its form (also in a disordered fashion). Therefore, α may be considered as a random variable, rather than a fixed constant. In Fig. 1 we show some schemes of such a quenched-disorder scenario, developed now. For HDPs driven by GWN this distributed α modification was considered in Ref. [47]. Namely, we prescribe α to obey a Gaussian distribution with mean α_0 and variance σ^2,

$$p(\alpha) = \frac{1}{\sqrt{2\pi}\sigma}\exp\left[-\frac{(\alpha-\alpha_0)^2}{2\sigma^2}\right]. \tag{4}$$

Figure 1 shows the influence of different σ on the diffusion coefficient $D(x)$ in different diffusion scenarios.

The driving Gaussian colored noise term $\xi(t)$ in Eq. (2) is now taken to be the Ornstein-Uhlenbeck (OU) process, which takes the form

$$\frac{d\xi(t)}{dt} = -\frac{1}{\tau}\xi(t) + \frac{1}{\tau}\dot{W}(t), \tag{5}$$

where τ is the correlation time, and $W(t)$ represents the standard Brownian motion, and $\dot{W}(t)$ is the Gaussian white noise. For a given initial position ξ_0, the solution of Eq. (5) is $\xi(t) = \xi_0 e^{-t/\tau} + \frac{1}{\tau}\int_0^t e^{-(t-s)/\tau} dW_s$. Thus, the correlation function yields in the form

$$\langle \xi(t)\xi(s)\rangle = \left(\langle \xi_0\rangle^2 - \frac{1}{2\tau}\right)e^{-\frac{1}{\tau}(t+s)} + \frac{1}{2\tau}e^{-\frac{1}{\tau}|t-s|}. \tag{6}$$

As the last ingredient for our study, we perform the following stratification of the medium into a layered system corresponding to quenched disorder. For each domain, its midpoint $x_{c,i}$ is selected as the origin in the local nonuniform diffusion process and in each layer the law Eq. (3) with the local value for α is employed. The domain periodicity (or the layer thickness) is denoted below as $2\delta x$. The shape of the resulting $D(x)$ changes with x for different α_0; see Fig. 1. Note that the domain center $x_{c,i} = (\ldots, -2, 0, 2, \ldots)\delta x$ is the region of slowest diffusion at $\alpha_0 = 1$, while for $\alpha_0 = -2$ it is the fastest diffusion region, compare Figs. 1(a) and 1(b).

Another important parameter to study is the domain periodicity, $2\delta x$ (stratification of the environment). At each domain boundary, a particle jumps from one domain to another, or (when the size of individual steps becomes of the order of δx) also over several layers at once.

To compute Eq. (2) numerically, we take the discrete form in the Itô sense, namely, taking the prepoint. We refer the reader here to Refs. [88,89] for the detailed investigation of implications of different stochastic calculi applied to HDPs. In short, for a stochastic differential equation one distinguishes Itô (prepoint) [90], Stratonovich (middle-point) [91,92], and Hänggi-Klimontovich (post-point, also called "kinetic") [87,93] conventions, see also Refs. [84–86,94–96] for more details and a recent overview. When $\xi(t)$

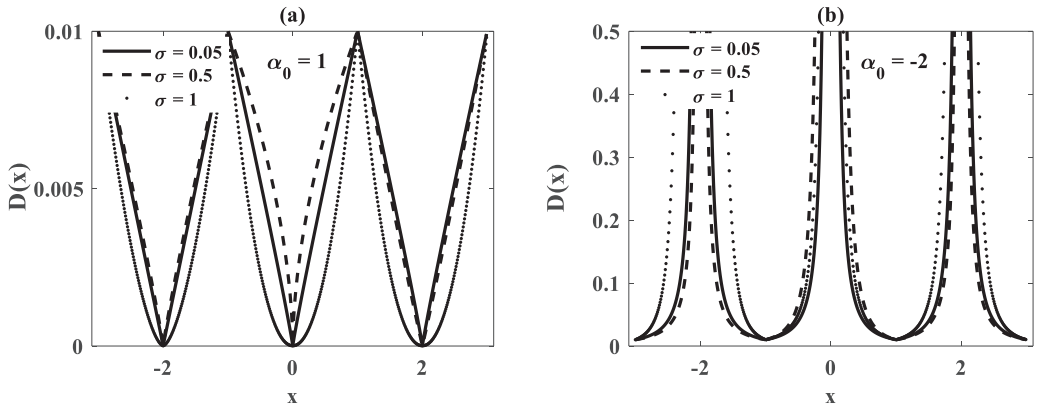

FIG. 1. Diffusion coefficient $D(x)$ for a stratified layered medium with local particle diffusion governed by HDPs. Panels (a) and (b) correspond to the cases of, respectively, $\alpha_0 = 1$ and $\alpha_0 = -2$. Other parameters are $\sigma = 0.05$, 0.5, and 1 (corresponding to very weak, intermediate, and strong disorder) and $\delta x = 1$ (meaning that $2\delta x$ is the domain periodicity). These values of parameters α_0 and σ are often used in the analysis below.

is a Gaussian white noise, for a system satisfying the fluctuation-dissipation theorem, Eq. (2) can achieve the desired Boltzmann distribution with the Hänggi-Klimontovich interpretation; while for systems with a constant friction coefficient and position-dependent diffusivity, Eq. (2) in the Itô interpretation turns out to be more appropriate [96]. In the current study, we consider $\xi(t)$ as an Ornstein-Uhlenbeck process, which is a second-order moment process with a continuous path. Thus, $\sqrt{2D(x)}\xi(t)$ is square-integrable for finite time, namely, it is equivalent to take any of these integral forms. With the second-order Runge-Kutta algorithm [97], the discrete form of Eqs. (2) and (5) is [97–99]

$$x(i+1) = x(i) + \Delta t[F_1(i) + F_2(i)]/2, \tag{7}$$

$$\xi(i+1) = \xi(i) + \Delta t[H_1(i) + H_2(i)]/2 + \sqrt{2\Delta t/\tau^2}\mu, \tag{8}$$

where $f(x,\xi) = \sqrt{2D(x)}\xi(t)$, Δt is the iteration step, and μ is a random number taken from the standard normal distribution. Here, the following notations are used

$$\begin{aligned} F_1(i) &= f[x(i), \xi(i)], \\ F_2(i) &= f[x(i) + \Delta t F_1(i), \xi(i) + \Delta t H_1(i)], \\ H_1(i) &= h[\xi(i)],\ H_2(i) = h[\xi(i) + \Delta t H_1(i)], \\ f[x(i), \xi(i)] &= \sqrt{2D[x(i)]}\xi(i),\ \ h\xi(i) = -\xi(i)/\tau. \end{aligned} \tag{9}$$

Based on this simulation algorithm, the influence of the model parameters τ, δx, and σ is investigated. In all simulations for each set of the model parameters we use the same time step $\Delta t = 0.1$, the length of the trajectories is $T = 10^4$ (each trace contains 10^5 simulation points), and the number of generated trajectories is $N = 10^3$.

III. MAIN RESULTS: PARTICLE SPREADING IN TERMS OF THE MSD AND TAMSD

A. Definition of the observables

We describe the spreading dynamics of a test particle for these stratified random-exponent HDPs using the concepts of MSD and TAMSD. The MSD is defined as the mean over the ensemble of diffusing particles [1,5–7,9],

$$\langle x^2(t)\rangle = \int_{-\infty}^{\infty} x^2 P(x,t)dx, \tag{10}$$

where $P(x,t)$ is the probability density function, while the TAMSD for the k th trajectory is defined as

$$\overline{\delta_k^2(\Delta)} = \frac{1}{T-\Delta}\int_0^{T-\Delta} [x_k(t+\Delta) - x_k(t)]^2 dt, \tag{11}$$

where Δ is the lag time and T is the total length of the trajectory. The mean over the ensemble of N independent TAMSD realizations (the ensemble-averaged TAMSD) is computed at every lag time according to

$$\left\langle \overline{\delta^2(\Delta)} \right\rangle = \frac{1}{N}\sum_{k=1}^{N} \overline{\delta_k^2(\Delta)}. \tag{12}$$

Therefore, the MSD involves averaging over space, while the TAMSD is based on a sliding-window of with Δ averaging along the trajectory. When the MSD and TAMSD are equal, for long observation times and for short lag times, i.e., when $\Delta/T \to 0$, the process is called ergodic [1,6,100,101],

$$\langle x^2(\Delta)\rangle = \lim_{\Delta/T\to 0} \overline{\delta^2(\Delta)}. \tag{13}$$

This formula combines the time- and ensemble-averaged views of a statistical observable.

B. The case of a fixed diffusivity scaling exponent in a single layer

To understand the impact of GCN, we list here some results for HDPs with a constant diffusivity exponent driven by GWN, as obtained in Refs. [40,47]. According to the general consideration, the MSD and mean TAMSD of HDPs follow the relations [40]

$$\begin{aligned} \left\langle x^2_{\mathrm{HDP+GWN}}(t)\right\rangle &= \frac{1}{\sqrt{\pi}}\Gamma\left(\frac{2}{2-\alpha}+\frac{1}{2}\right) \\ &\times \left[2\Big/\left(\frac{2}{2-\alpha}\right)\right]^{2\,\frac{2}{2-\alpha}} (D_0 t)^{\frac{2}{2-\alpha}} \propto t^{\frac{2}{2-\alpha}}, \end{aligned} \tag{14}$$

and

$$\overline{\langle \delta^2_{\mathrm{HDP+GWN}}(\Delta)\rangle} = \langle x^2_{\mathrm{HDP+GWN}}(\Delta)\rangle \left(\frac{\Delta}{T}\right)^{1-\frac{2}{2-\alpha}} \propto \Delta^1, \quad (15)$$

correspondingly. We immediately note the difference in the scaling exponents of the MSD and mean TAMSD and the apparent nonergodicity of this system [40]. For $\alpha = 0$ the MSD was shown to coincide with the mean TAMSD (pure Brownian diffusion). For $\alpha = 1$ the MSD was found to be smaller in magnitude than the mean TAMSD and to grow superdiffusively, Eq. (14). For $\alpha = -2$, on the contrary, the MSD is larger in magnitude than the mean TAMSD and grows subdiffusively. Remarkably, for all three choices of the scaling exponents of $D(x)$ the mean TAMSD was shown to grow strictly linearly with lag time, as predicted by Eq. (15) (only the TAMSD prefactor is a function of α). This MSD versus TAMSD discrepancy gave rise to the phenomenon of weak ergodicity breaking for standard HDPs [40,41,47]. It was also demonstrated [47] that the nonergodic behavior of standard HDPs is remarkably similar to that of continuous-time random walks [10,70,101], as is their aging behavior [40,41,102].

As we show below, the values of the model parameters σ and δx strongly impact the magnitudes and characteristic features of the MSD and TAMSD. In what follows, we report the new properties for HDPs with GCN in stratified environments and compare the results to nonstratified HDPs driven by GWN. First, we obtain some scaling relations for the MSD and mean TAMSD for HDPs driven both by GWN and GCN. Starting with the standard HDP [40,47], the MSD scaling of

$$\langle x^2_{\mathrm{HDP+GWN}}(t)\rangle \sim C(\alpha) t^{\frac{2}{2-\alpha}} \propto t^{\frac{2}{2-\alpha}}, \quad (16)$$

where $C(\alpha) = [(\frac{2-\alpha}{2})^2 2D_0]^{\frac{2}{2-\alpha}}$. This differs only by an α-dependent prefactor from the exact solution Eq. (14). For the TAMSD computed at short lag times ($\Delta \ll T$) using Eq. (16), one gets in the leading order the relation between the MSD and mean TAMSD identical to Eq. (15). We employ the same method for HDPs driven by GCN. For this process with $D(x)$ = const, the MSD follows the Ornstein-Uhlenbeck law [9],

$$\begin{aligned}\langle x^2_{\mathrm{GCN}}(t)\rangle &= 2D_0 \int_0^t \int_0^t \langle \xi(t')\xi(t'')\rangle dt' dt'' \\ &= 2D_0 \int_0^t \int_0^t \left[\left(\langle \xi_0\rangle^2 - \frac{1}{2\tau}\right) e^{-\frac{1}{\tau}(t'+t'')} \right. \\ &\quad \left. + \frac{1}{2\tau} e^{-\frac{1}{\tau}|t'-t''|}\right] dt' dt''. \end{aligned} \quad (17)$$

If we take ξ_0 as a fixed constant $\xi_0 = 0$, then $\langle \xi_0\rangle^2 = 0$, and the formula can be simplified as

$$\begin{aligned}\langle x^2_{\mathrm{GCN}}(t)\rangle &= \frac{D_0}{\tau} \int_0^t \int_0^t \left[e^{-|t'-t''|/\tau} - e^{-(t'+t'')/\tau}\right] dt' dt'' \\ &= D_0\left(4\tau e^{-\frac{t}{\tau}} - \tau e^{-\frac{2t}{\tau}} + 2t - 3\tau\right). \end{aligned} \quad (18)$$

In this case, at short times, i.e., $t \ll \tau$, expanding Eq. (18) around zero with scale t/τ yields

$$\langle x^2_{\mathrm{GCN}}(t)\rangle \approx \frac{2D_0 t^3}{3\tau^2}. \quad (19)$$

For the long-time behavior, i.e., $t \gg \tau$, the exponential parts in Eq. (18) vanish and the MSD becomes $\langle x^2_{\mathrm{GCN}}(t)\rangle \approx 2D_0 t$, which is independent of the correlation time τ.

If we take ξ_0 as a random number, and let it satisfy the equilibrium distribution of the OU process, i.e., $\xi_0 \sim N(0,\ 1/\sqrt{2\tau})$, then the MSD can be simplified as

$$\begin{aligned}\langle x^2_{\mathrm{GCN}}(t)\rangle &= \frac{D_0}{\tau} \int_0^t \int_0^t e^{-|t'-t''|/\tau} dt' dt'' \\ &= 2D_0 t\left[1 - \frac{\tau}{t}\left(1 - e^{-\frac{t}{\tau}}\right)\right]. \end{aligned} \quad (20)$$

In this case, at short times, i.e., $t \ll \tau$, analogously,

$$\langle x^2_{\mathrm{GCN}}(t)\rangle \approx \frac{D_0 t^2}{\tau}. \quad (21)$$

For the long-time behavior, the MSD is always $\langle x^2_{\mathrm{GCN}}(t)\rangle \approx 2D_0 t$.

Thus, at short times the MSD is sensitive to the initial value ξ_0 of the OU process, which will change the power of the MSD scaling. However, although the correlation time τ also affects the short-time behavior significantly, it does not affect the scaling exponent of the long-time behavior. In addition, τ has no influence on the long-time behavior for $\alpha = 0$. Analogously, for other α the long-time behavior mainly depends on the quenched disorder, i.e.,

$$\langle x^2_{\mathrm{HDP+GCN}}(t)\rangle \sim C(\alpha) t^{\frac{2}{2-\alpha}}, \quad (22)$$

which is corroborated in the following figures.

The results of simulations for different α under the conditions of both fixed and random initial position ξ_0 are presented in Fig. 2. We target here the scaling behavior of the particle displacements and are aware of the fact that the α-dependent prefactors of these scaling relations (not predicted correctly by the scaling-based analytical estimations above) cause the discrepancy in the magnitude between theory and simulations. We mention that in Figs. 2(a)–2(c), the initial value ξ_0 of the OU process is fixed as $\xi_0 = 0$, while in Figs. 2(d)–2(f) ξ_0 is random and satisfying $\xi_0 \sim N(0,\ 1/\sqrt{2\tau})$, which is the steady state distribution of Eq. (5). In addition, to highlight the short-time behavior for the case $\alpha = -2$, we take $x_0 = 0.7$ away from the origin point.

At $\alpha = 0$, the spread of individual TAMSD realizations is very small at short lag times (reflecting very reproducible particle displacements) and it increases due to worsening statistics at longer lag times (the standard cone-like scatter of TAMSDs). Moreover, the theoretical short-time MSDs, i.e., Eqs. (19) and (21), are in good agreement with simulations for both fixed $\xi_0 = 0$ and random ξ_0. This phenomenon indicates that the MSD is indeed sensitive to the initial value of the OU process. For $\xi_0 = 0$ in Fig. 2(b), the MSD increases with the power 3, which is faster than the power 2 for $\xi_0 \sim N(0,\ 1/\sqrt{2\tau})$ in Fig. 2(e). In addition, for the long-time behavior the predicted result MSD $= 2D_0 t$ also agrees well with the simulation results, which is consistent with the conjecture Eq. (22) for all α.

At $\alpha = -2$, the MSD features some "jumps" at short times and the spread of individual TAMSDs is significant both at short and at long lag times. We observe some trajectories that exhibit large jumps from the region of large diffusivity (near

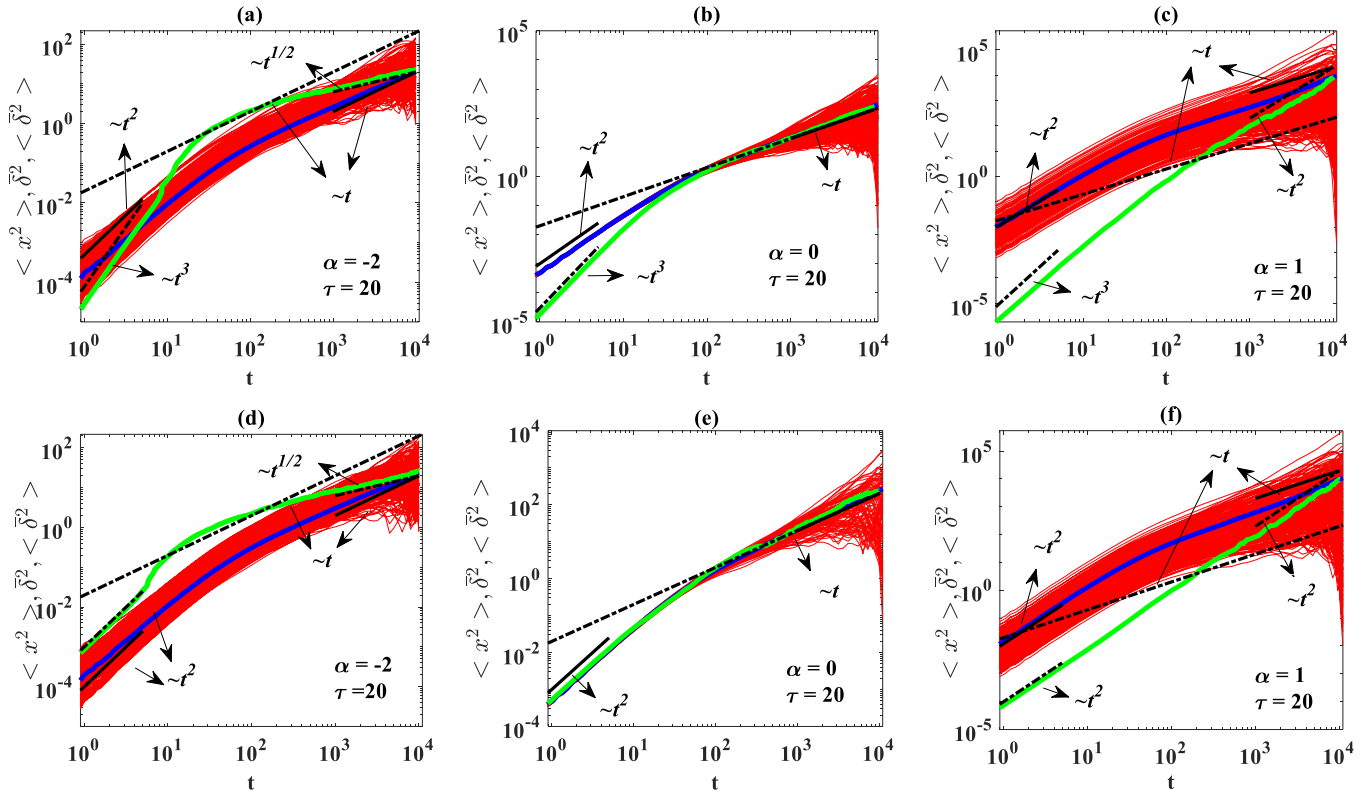

FIG. 2. MSD, individual TAMSDs, and mean TAMSD for the unconfined HDPs with constant α-exponents driven by GCN, plotted for different values of the scaling exponent of the diffusion coefficient (values provided in the plots) as function of diffusion time. Here, as well as in other plots, the MSDs $\langle x^2(t)\rangle$ are the thick green curves, the individual TAMSDs $\overline{\delta_k^2(\Delta)}$ are the red lines, and the mean TAMSDs $\langle\overline{\delta^2(\Delta)}\rangle$ are the thick blue curves. The MSD asymptotes at short and long times as well as the TAMSD asymptote are the dashed and solid lines, respectively. The black dot-dashed line is the Brownian asymptote, $\langle x^2(t)\rangle = 2D_0t$. In panels (a)–(c), the initial position of the OU process is taken as a fixed constant $\xi_0 = 0$. In panels (d)–(f), the initial position ξ_0 is a random number satisfying the equilibrium distribution of the OU process Eq. (5), i.e., $\xi_0 \sim N(0,\ 1/\sqrt{2\tau})$. In panels (a), (d), to make the slope of MSD clear, we assume $x_0 = 0.7$, while in panels (b), (c), (e), (f), $x_0 = 0.1$. In all the figures, the relaxation time is $\tau = 20$.

$x = 0$ for this value of α) to the region of small diffusivity (far from $x = 0$) and "get stuck" there. This gives rise to dramatic jumps in the final MSD at these time instances and to some rather stalled individual TAMSD trajectories. However, these "jumps" will make it difficult to distinguish the slope of the MSD, thus we choose merely trajectories without "jumps" within $T = 10^4$ in Fig. 2 to clearly present the power.

We observe that at short times the TAMSD is close to ballistic for $\alpha = 0$, 1, and -2 in both cases of $\xi_0 = 0$ and $\xi_0 \sim N(0,\ 1/\sqrt{2\tau})$. However, the short-time MSD scaling is cubic in case of fixed $\xi_0 = 0$ and ballistic in case of random $\xi_0 \sim N(0,\ 1/\sqrt{2\tau})$ for all $\alpha = 0$, 1, and -2. This phenomenon indicates that α almost has no influence on the short-time scaling, where the OU process plays the key role. Particularly, the initial value ξ_0 is able to change the power of the MSD scaling, while the correlation time τ only changes its starting value. Moreover, at long times, we find that the mean TAMSD and MSD are roughly linear for $\alpha = 0$, while the MSD is subdiffusive for $\alpha < 0$ and superdiffusive for $\alpha > 0$, as expected in Eq. (22). At the last point of the trajectory the MSD is equal to the mean TAMSD, as they should. In particular, both simulations and the conjecture Eq. (22) show that the MSD scaling at long times does not depend on the correlation time. The only effective factor is the exponent index α. This can be explained by viewing the OU process as a white correlated process in the scale of τ when t is large enough. Thus, at the long-time limit $D(x)$ functions as the main effective factor.

In Fig. 2 we show the Brownian asymptote to be able to assess whether the diffusion for HDPs with GCN is enhanced or suppressed compared to the Brownian limit in a single layer. The correlation time τ shows a significant influence on the MSD at short times; however, it does not affect the long-time behavior. With different exponent index α, the MSD and mean TAMSD correspond to subdiffusion, normal diffusion and superdiffusion with respect to $\alpha = -2$, 0, and 1. Next, we determine the exact effects of GCN and a stratified medium on the HDPs.

C. The case of distributed scaling exponent of the diffusivity: Effects of correlation time τ of GCN

In this section, we analyze the influence of the GCN correlation time τ on the diffusive behavior and characteristics of particles in a stratified medium when the local dynamics is governed by random-exponent HDPs. In all the following figures in this section, the initial value of the OU process is fixed $\xi_0 = 0$. Note that trajectories with "jumps" are specifically considered in these figures.

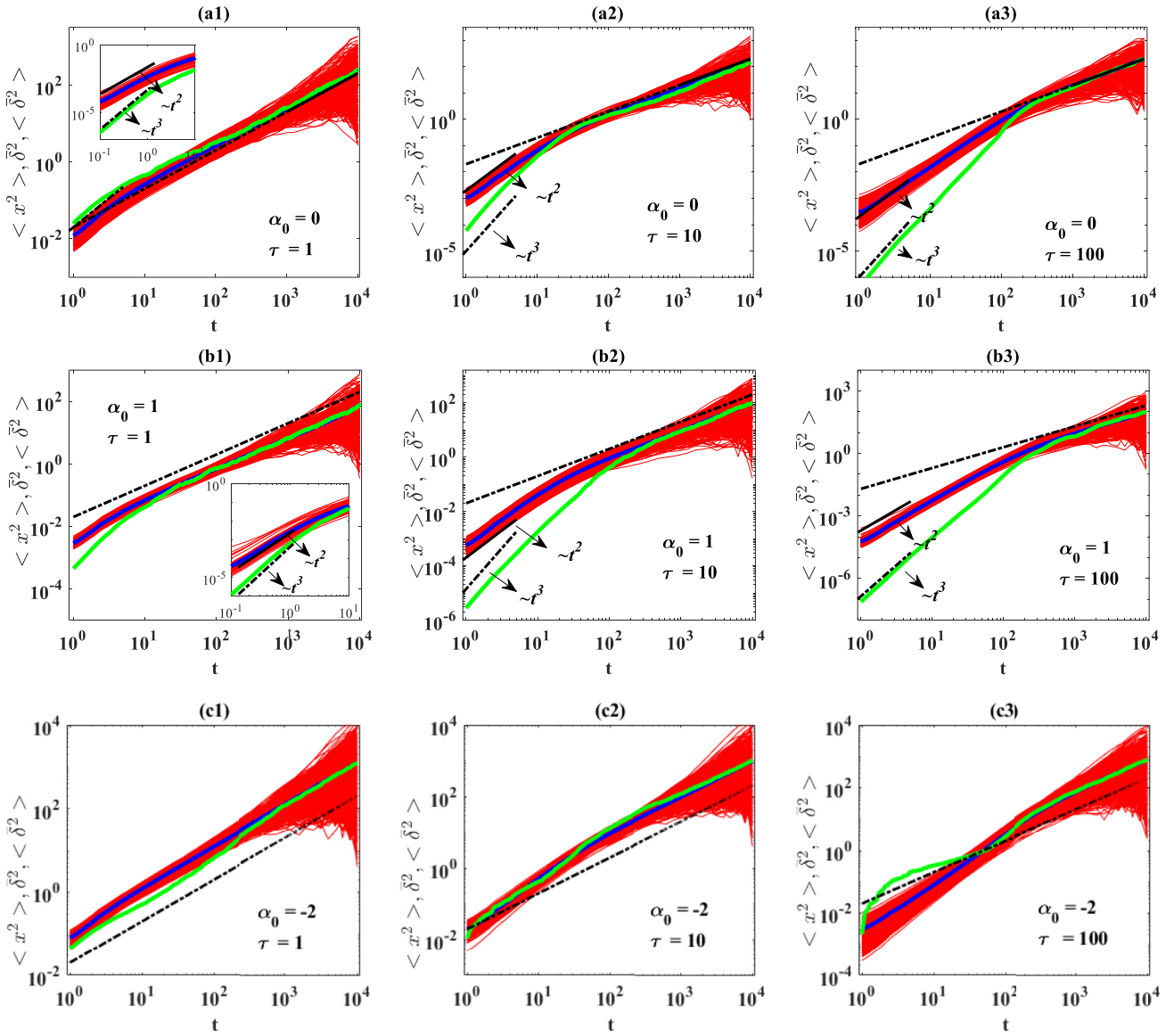

FIG. 3. Dynamic characteristics of particles obeying stratified HDPs with random exponents diffusing in a medium with a quenched disorder. Panels (a)–(c) show stratified HDPs with mean diffusivity exponent $\alpha_0 = 0,\ 1,\ -2$, respectively. The graphs are plotted by systematically varying τ, as indicated in the plots. The black dot-dashed line is the Brownian asymptote, $\langle x^2(t)\rangle = 2D_0 t$. Other parameters: variance of the HDP exponent variation $\sigma = 1$, domain periodicity of the medium $\delta x = 1$, initial particle position $x_0 = 0.1 + \delta x$ (as in Refs. [47]), and $\xi_0 = 0$. We fix the constants $D_0 = 0.01$ and $D_{\rm off} = 0.001$ throughout the paper. The notations for curves and lines are the same as described in the caption of Fig. 2.

Before describing the Fig. 3 in detail, let us take a brief glance at the whole picture. It is obvious that τ should not affect the long-time behavior for any α: No matter how τ changes the system will eventually perform normal diffusion at sufficiently long times. The only difference is that the effective diffusion coefficient varies with α. Thus, when we only consider the long-time dynamics, Eq. (2) driven by GCN can be reduced to the simple Gaussian white noise case, namely, $dx(t)/dt = \sqrt{2D(x)}W(t)$. In a multilayer medium, particles will jump between adjacent layers and induce a multimodal PDF [47]. If we view each layer as a point, then two adjacent layers corresponds to two point with a distance of $2\delta x$. Then the HDP in the stratified medium reduces to a random walk process. We give each point a label symmetric about the origin and assume that a particle at the k th point will jump to the (k-1)th and ($k+1$)th points with equal probability 1/2. Particularly, a successful jump either to the left or right has a rate λ, which corresponds to the steady state escape rate from the middle point of a layer to its adjacent layers. Then the change of the probability that a particle stays at the k th layer comes from the input from and output to its adjacent layers. Then we can write the master equation as

$$\frac{dp_k(t)}{dt} = \frac{1}{2}\lambda p_{k-1}(t) + \frac{1}{2}\lambda p_{k+1}(t) - \lambda p_k(t). \tag{23}$$

From this we obtain the mean $\langle x(t)\rangle$, and the MSD as

$$\langle x(t)\rangle = \sum_{k=-\infty}^{+\infty} (2k\delta x)p_k(x) = 0, \tag{24}$$

by symmetry, and

$$\langle x^2(t)\rangle = \sum_{k=-\infty}^{+\infty} (2k\delta x)^2 p_k(x). \tag{25}$$

The MSD can be solved in the form

$$\begin{aligned}\frac{\mathrm{d}\langle x^2(t)\rangle}{dt} &= \sum_{k=-\infty}^{+\infty} (2k\delta x)^2 \frac{dp_k(t)}{dt} \\ &= 4\lambda\delta x^2 \sum_{k=-\infty}^{+\infty} k^2\left(\frac{1}{2}\lambda p_{k-1}(t) + \frac{1}{2}\lambda p_{k+1}(t) - \lambda p_k(t)\right) \\ &= 4\lambda\delta x^2 \sum_{k=-\infty}^{+\infty} p_k(t) \\ &= 4\lambda\delta x^2. \end{aligned} \tag{26}$$

Thus, the MSD is

$$\langle x^2(t)\rangle = 4\lambda\delta x^2 t. \tag{27}$$

It should be emphasized that although the analysis is based on a fixed α, the result has direct significance even for random α. We find that $\langle x^2(t)\rangle = 4\lambda\delta x^2 t$ is consistent with the numerical results in Figs 3–5, that after passing many layers, the system performs normal diffusion and the effective diffusion coefficient is $D_{\mathrm{eff}} = 2\lambda\delta x^2$. Therefore, the key to determine D_{eff} is finding the escape rate λ. Generally, λ can be given by the inverse of the mean first passage time T, that a particle starts from the middle of a layer and reaches either middle point of its adjacent layers.

When $D(x) = D_0$, it is known that $\lambda = D_0/2\delta x^2$, thus the MSD is $\langle x^2(t)\rangle = 2D_0 t$. This is analogous to the classic result. When $\alpha \neq 0$, the mean first passage time can be obtained by solving the Pontryagin equation [112], which is given in the appendix in detail. Note that the theoretical result from the Pontryagin expression is valid for small $|\alpha|$ when $D(x)$ changes slowly. When $|\alpha|$ is large, $D(x)$ changes quickly and this approach cannot be applied. Thus, for large $|\alpha|$, we generate λ by numerical simulation, while for small $|\alpha|$, we use theoretical results from the Pontryagin equation.

We start with the simplest situation of $\alpha_0 = 0$ (little variation of the diffusivity in space due to $\langle\alpha\rangle = 0$). In panel (a1) of Fig. 3 we observe that when τ is relatively small ($\tau = 1$), the diffusion characteristics change only slightly as compared to the nonlayered system and pure Brownian diffusion. Namely, the spread of the TAMSDs increases slightly, while the deviations in the magnitude of the MSD and mean TAMSD from the Brownian asymptote only occur at short times (in the regime $t \lesssim \tau$). As the noise correlation time increases to $\tau = 10$ and $\tau = 100$ in Figs. 3(a2) and 3(a3), respectively—the MSD and mean TAMSD are reduced significantly in their magnitude at short times ($\{t, \Delta\} \lesssim \tau$). The MSD drop is particularly pronounced and the MSD scaling is more superdiffusive (as compared to that of the TAMSD) in the short-time regime. This drop in the MSD and mean TAMSD magnitudes is similar to the trends observed for free HDPs driven by GCN at $\alpha = 0$, for which Eq. (19) shows that the MSD depends sensitively on τ. For example, the MSD of $\tau = 1$ is 10^4 times that of $\tau = 100$ at short times, also see Figs. 2(b) and 2(e). Both the MSD and mean TAMSD in this time domain reveal superdiffusive behaviors (the scaling of the mean TAMSD is approximately ballistic at short times for $\alpha_0 = 0,\ 1$). At much longer times, after the diffusing particles cross a large number of layers, the MSD and mean TAMSD magnitudes start following the Brownian asymptote $\langle x^2(t)\rangle = 2D_0 t$. The spread of individual TAMSD realizations changes only slightly with increase of τ for the case $\alpha_0 = 0$, both at short and long lag times. For long correlation times, as in Fig. 3(a3), it becomes visible that the MSD and mean TAMSD (respectively, the green and blue curves in Fig. 3) feature generally two regimes: the domain of fast growth at short times and steady growth at long times.

For $\alpha_0 = 1$ we observe very similar trends with variation of the correlation time in the range $\tau = 1,\ 10,\ 100$, as we observed for $\alpha_0 = 0$; see, respectively, Figs. 3(b1)–(b3). The only detectable differences are that the spread of individual TAMSDs becomes slightly smaller than for $\alpha_0 = 0$ (but almost does not change with τ) and significantly smaller than for free HDPs driven by GCN, as analyzed in Fig. 2. Also, varying τ from $\tau = 1$ to $\tau = 100$ the magnitudes of the MSD and mean TAMSD progressively decrease compared to the Brownian asymptote; the effect is particularly pronounced at short lag times. The MSD and mean TAMSD are superdiffusive at short times and their behavior turns fully Brownian with nearly equal magnitudes at long times (after particles cross many layers of this stratified medium). As given by Eq. (27) and the Appendix, the MSD for the long-time behavior is $\langle x^2(t)\rangle = \frac{2D_0\delta x}{\ln(2\delta x)-1}t$ for fixed $\alpha = 1$. This approximation is only valid for large δx [see Figs. 4(b2), 4(b3), and 11(c)], while for $\delta x = 1$ in Fig. 3, it actually loses its validity. However, we numerically calculate λ and presents the result $\langle x^2(t)\rangle = 4\lambda\delta x^2 t$ in the figure, which fits well the simulation results. Note that although Eq. (27) is for deterministic α, it also works well for random α with a small σ. Moreover, the MSD and mean TAMSD are always below the Brownian-motion asymptote. In particular, for long correlation times it is apparent that the MSD and mean TAMSD magnitudes are very different (both in scaling and magnitude) at short times (indicating the nonergodic behavior), while at long times the system behaves ergodically [3,6,8], with MSD $(t) \sim$ TAMSD (t).

For $\alpha_0 = -2$ the behavior of the system is similarly ergodic at long times, with the MSD and mean TAMSD magnitudes significantly above the Brownian asymptote, see Figs. 3(c1)–(c3). The result $\langle x^2(t)\rangle = 4\lambda\delta x^2 t$ fits well with the long-time MSD. At short times the discrepancy between the MSD and mean TAMSD increases slightly for larger values of τ. In other words, the shorter the correlation time τ, the more ergodic the overall particle diffusion at short times becomes. We emphasize here that the approximation $\langle x^2(t)\rangle = 4\lambda\delta x^2 t$ is always valid, but it is difficult to give an effective expression of the escape rate λ when $|\alpha|$ is large. This can be verified by Figs. 11(e) and 11(f), where λ is obtained numerically.

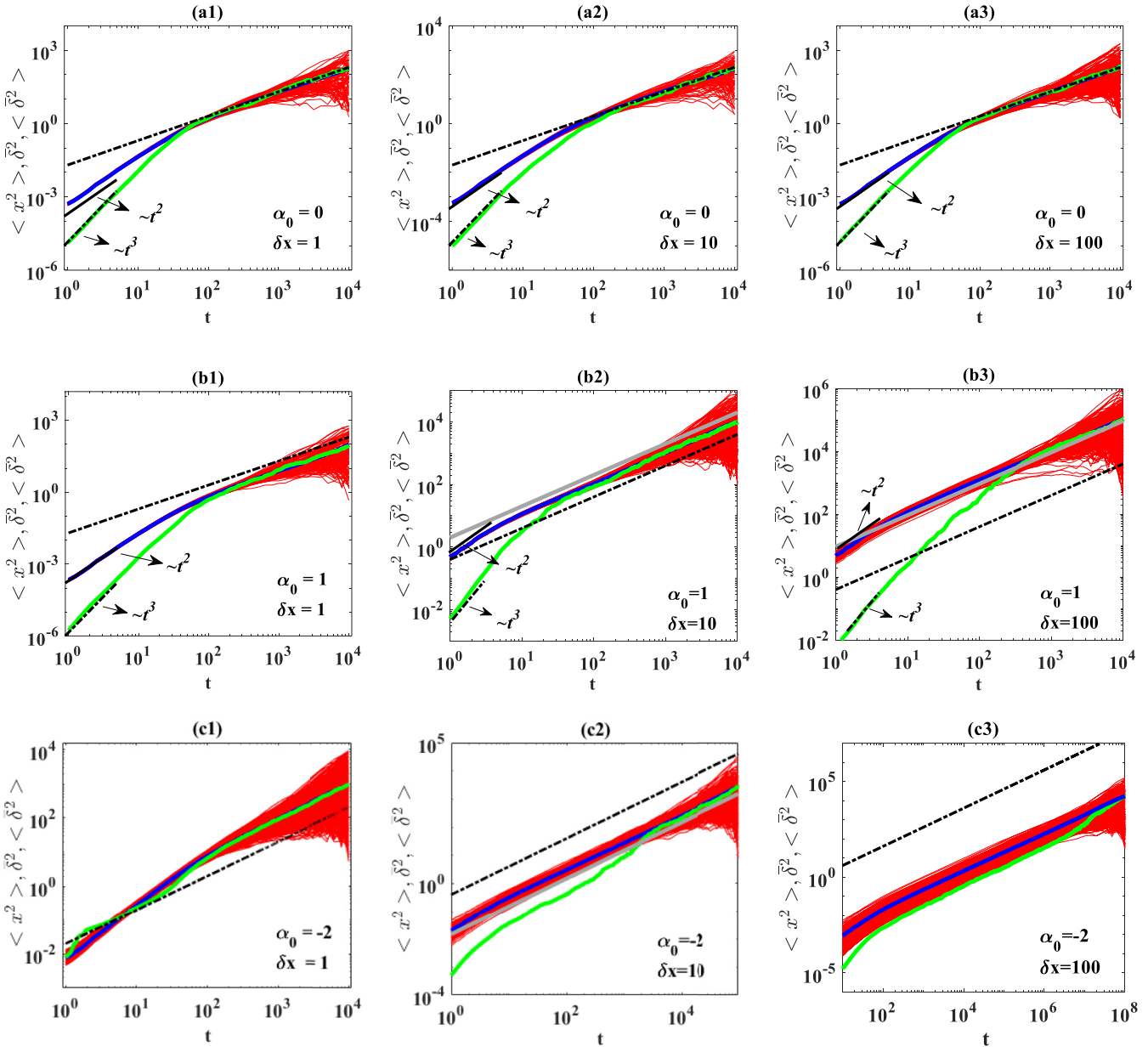

FIG. 4. The same as described in the caption of Fig. 3, with the same notations for different curves and asymptotes, plotted for three values of the scaling exponents of $D(x)$ and for varying layer thickness, $\delta x = 1$, 10, and 100. Note that in Figs. 3(c1)–3(c3) the initial position is taken as $x_0 = 0.1$ and $D_0 = 0.2$. The gray lines correspond to Eq. (A2) or Eq. (27). In panel (c3) the gray line is not given because the corresponding mean first exit time is too large to compute its exact value. Parameters: $\sigma = 0.05$, $\tau = 20$, and $\xi_0 = 0$.

D. Distributed scaling exponents: Effects of varying layer thickness δx

Below, we analyze the influence of the domain periodicity of stratified GCN-driven HDPs on the MSD and mean TAMSD behavior as well as on the spread of individual TAMSDs.

For $\alpha_0 = 0$ the varying domain periodicity essentially has no visible effect because for the relatively small spread of scaling exponents of the diffusivity ($\sigma = 0.05$) the system appears almost homogeneous, see Figs. 4(a1)–4(a3), so that the trends we observe are identical to those for free HDPs driven by GCN, see Fig. 2(b). As one can see, even at the longest time we have in the simulations the squared displacements of the particles are considerably around or smaller than δx^2 for relatively large δx, so the particles stay mostly in the same layer of the medium in this case. Thus, it is natural that the varying periodicity does not affect the system's behavior for $\alpha_0 = 0$.

For $\alpha_0 = 1$ we observe that at $\delta x = 100$ the behavior of the system is similar to that for free HDPs driven by GCN, compare Fig. 4(b3) and Fig. 2(c). But Fig. 4(b3) tends to normal diffusion, while in Fig. 2(c) the MSD is proportional to t^2 at long times. When δx is large, the result $\langle x^2(t)\rangle = \frac{2D_0\delta x}{\ln(2\delta x)-1}t$ is valid as shown in the figure. It can be seen from the effective

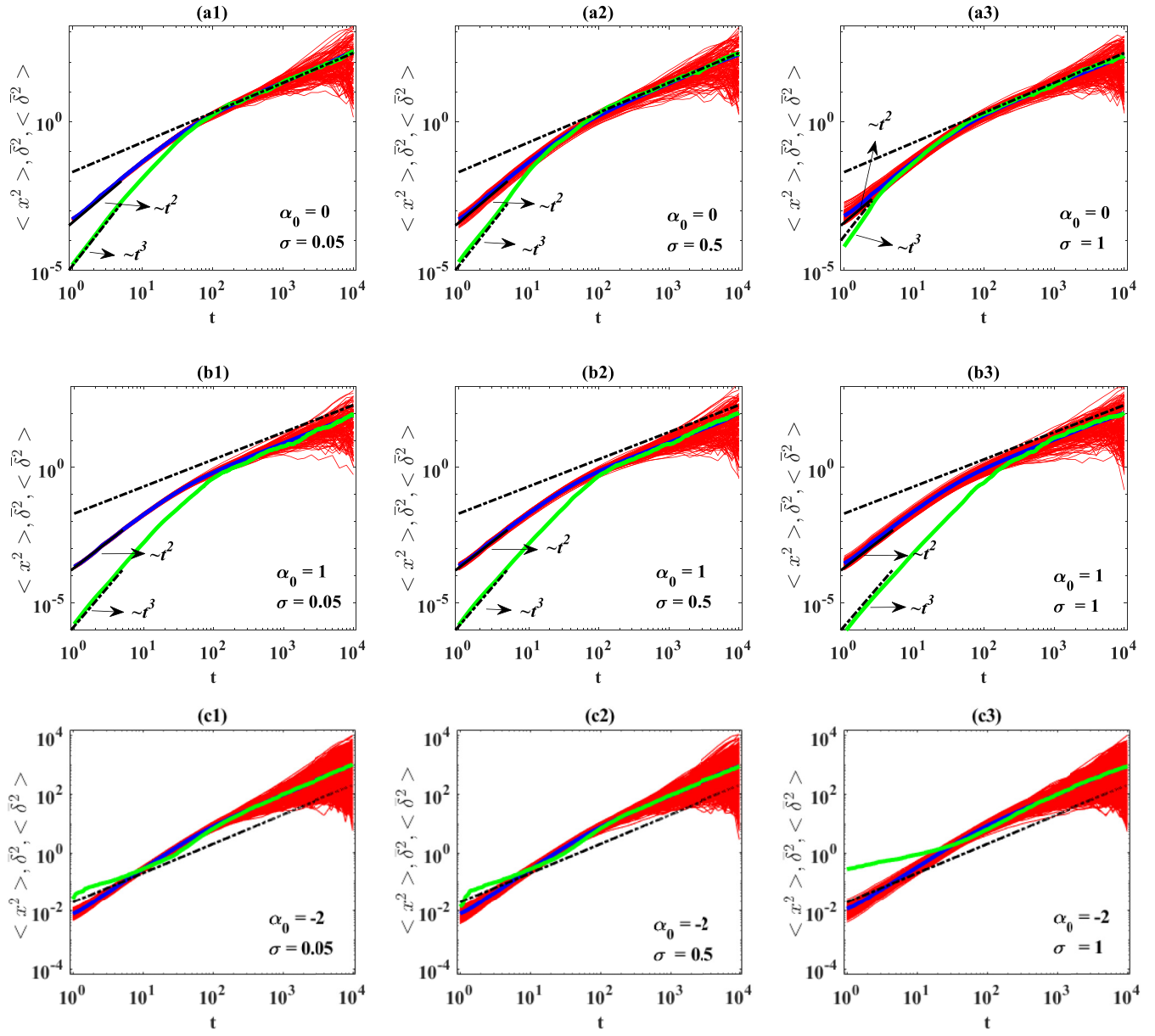

FIG. 5. Particle-diffusion characteristics for HDPs with GCN in a quenched-disorder medium plotted for different variance σ of the scaling-exponent distribution $p(\alpha)$; see Eq. (4). Parameters: $\delta x = 1$, $\tau = 20$, and $\xi_0 = 0$. The notations for curves and lines are the same as described in the caption of Fig. 3.

diffusion coefficient $D_{\rm eff} = \frac{D_0 \delta x}{\ln(2\delta x)-1}$ that $D_{\rm eff}$ increases with δx for large δx. Therefore, as the layer thickness δx decreases, the magnitudes of the MSD and mean TAMSD in the entire range of diffusion times drop significantly. At $\delta x = 1$ the long-time MSD and mean TAMSD magnitudes drop below the Brownian asymptote. Consequently, with decreasing δx the diffusion distances of the particles become shorter and the spreading dynamics is impeded. In stark contrast, the MSD magnitude at short time stays almost unaffected by varying δx values. We detect that the long-time domain, where the MSD is nearly equal to the mean TAMSD, becomes progressively large as the δx values decrease and more separate layers of this stratified system are visited by diffusing particles. We also observe the prominent trend of a considerable narrowing of the distribution of individual TAMSDs with decreasing periodicity δx; see Figs. 4(b1)–4(b3). This "shrinkage" tendency is similar to the trend detected previously for standard HDPs driven by GWN; see Fig. 4 of Ref. [47].

For $\alpha_0 = -2$, we find that for smaller δx values the range of times for which our computer simulations yield close results for the MSD and the mean TAMSD increases. Specifically, at $\delta x = 100$ we find a pronounced MSD versus mean TAMSD discrepancy for the entire range of times simulated (except for the very last point of the trajectory), while at $\delta x = 1$ the simulations reveal that the MSD is very close to the mean TAMSD almost in the entire domain of observation times.

We mention a nonsmooth, spiky behavior of the MSD at large δx, stemming from particles displaced from the region of extremely high diffusivity into the region of low diffusivity (in the tail of $D(x)$ distribution) in a single heterogeneous domain. A single trajectory with a large position jump of this kind can ultimately give rise to a nonsmooth, jumpy behavior for the MSD. For small δx, the particles cover many layers in the stratified medium and jump between the adjacent diffusivity domains rather frequently. This leads to averaging of the heterogeneities of the diffusion coefficient and diffusion takes place effectively like in a uniform or homogenized environment. This results in nearly equivalent magnitudes of the MSD and mean TAMSD in the long-time limit for small medium periodicities and diffusion appears nearly ergodic for long times.

The role of the layer periodicity $2\delta x$ has a decisive effect on the diffusion properties. For small values of $2\delta x$ the particles rapidly explore the layer containing the initial position. Relatively early the particle then crosses to the vicinal layers. After several "barrier crossings" normal, ergodic diffusion with an effective diffusion constant emerges. For large $2\delta x$ the particle initially only explores the layer it was seeded in and does not feel the layering geometry. The amplitude spread of the TAMSDs is pronounced, as is the nonergodic behavior, the inherent characteristics of HDPs at $\alpha_0 \neq 0$ driven both by GWN and GCN.

E. Distributed scaling exponents: Dependence on the variance σ of the distribution $p(\alpha)$ of the diffusivity scaling exponents

We now present the results for varying spread σ of the scaling exponents α of $D(x)$, see Eq. (4). In Fig. 5 the results of computer simulations are presented for a rather small layer periodicity $\delta x = 1$ and for the GCN correlation time $\tau = 20$.

For $\alpha_0 = 0$ and rather small values of σ we do not observe any detectable change from the behavior of free HDPs with GCN, comparing Fig. 5(a1) and Fig. 2(b). This is because when σ is small, the exponent α will be so small that $D(x)$ changes slightly within the domain $(-\delta x, \delta x)$. As the variance increases to $\sigma = 0.5$ and $\sigma = 1$ individual TAMSDs acquire a larger spread, but the overall MSD and mean TAMSD behaviors and their magnitudes remain quite similar to the case of small σ. When we increase δx, the spread will be even larger with increasing σ, but the long-time behavior will remain unchanged. The only visible difference is the increase of the MSD magnitude at short times for the case $\sigma = 1$. Specifically, the long-time domain (at $t \gg \tau$) where the MSD becomes nearly equivalent to the mean TAMSD (and to the standard Brownian asymptote) remains nearly unchanged. This long-time ergodic behavior is, however, complemented by the nonergodicity at short times where the magnitudes of the MSD and mean TAMSD are observed to be substantially different, in particular for small-to-moderate σ values [see Figs. 5(a1) and 5(a2)].

For $\alpha_0 = 1$ we also observe that the initial and final values of both the MSD and mean TAMSD do not change much with σ (for its variation in the range chosen here). The scatter of individual TAMSDs increases with σ and the magnitude of the effect is similar to that observed for $\alpha_0 = 0$ case. The difference is in the fact that the MSD and mean TAMSD magnitudes for $\alpha_0 = 1$ are always below the Brownian asymptote. In the long-time limit ergodic behavior is realized.

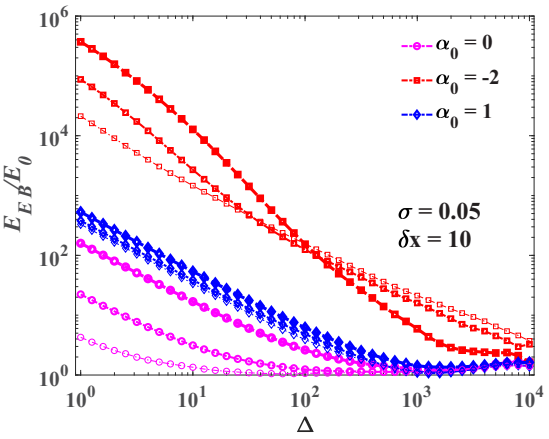

FIG. 6. Ergodicity breaking parameter, normalized to the reference behavior for Brownian motion, E_{EB}/E_0, plotted as function of lag time, Δ. The colors of symbols are specified in the legend. The line types from thin to thick correspond to $\tau = 1$, 10, and 100, respectively. Other parameters are $\sigma = 0.05$, $\delta x = 10$, and $\xi_0 = 0$.

In the case $\alpha_0 = -2$, likewise, the initial and final values of the MSD and mean TAMSD almost do not change with σ (the MSD becomes larger only when $\sigma = 1$) and the amplitude scatter of individual TAMSDs becomes somewhat larger as σ grows. The same trend is observed in Figs. 5(a) and 5(b) for $\alpha_0 = 0$ and $\alpha_0 = 1$, respectively. As compared to the situation $\alpha_0 = 1$, the MSD and mean TAMSD magnitudes are above the Brownian asymptote at long times. The results of simulations also reveal that at smaller σ the time domain where the MSD nearly coincides with the mean TAMSD is larger. The nearly ergodic behavior realized in this domain, thus, occupies a larger portion of the time domain employed in our computer simulations (see also the ergodicity analysis in Fig. 6 below).

It should be emphasized that for a small $\delta x = 1$ shown in Fig. 5, the influence of σ is small. But it will be different for a large δx, where $D(x)$ changes significantly. Moreover, when $|\alpha_0| > 3\sigma$, the sign of the exponent α is left almost unchanged, and the influence of σ is small. However, for $|\alpha_0| < 3\sigma$, the sign of α switches between negative and positive, which will induce a significant difference.

IV. RESULTS: ERGODICITY BREAKING AND NON-GAUSSIANITY

A. Definition of the observables

In recent years, nonergodic dynamics have been observed in a number of cellular and biological systems [3,6]. For instance, it was detected in the short-time motion of submicron particles in living yeast cells [11], single-particle diffusion on the surface of cell membranes [103,104], blinking dynamics of quantum dots [105,106], diffusion of granules and internal vacuoles [107], as well as of artificial tracers inside living cells [3,5,9–11,14,26]. The indicators of nonergodicity help us to determine the type and statistical characteristics of the measured observables for a given diffusion process. One of

them is the ergodicity breaking parameter. It is defined as the ratio of the relative variance and the TAMSD at a given lag time Δ [1,6,10,11,75],

$$E_{\rm EB}(\Delta) = \lim_{\Delta/T\to 0} \frac{\langle \overline{\delta^2(\Delta)}^2 \rangle}{\langle \overline{\delta^2(\Delta)} \rangle^2} - 1. \tag{28}$$

This parameter characterizes the degree of irreproducibility and quantifies relative spread of individual TAMSD realizations. For classical Brownian motion one obtains [3,75,76,108,109]

$$E_0(\Delta) = \frac{4\Delta}{3T}, \tag{29}$$

which means that the process is fully reproducible at long measurement times. Even for simple Brownian motion $E_0(\Delta)$ approaches zero asymptotically as $\Delta/T \to 0$ and vanishes only at vanishing lag-time values. This says that fluctuations may be relevant for finite Δ/T values. Another nonergodicity characteristic is the ratio of the mean TAMSD to the MSD [47,110],

$$E_{\rm NE}(\Delta) = \frac{\langle \overline{\delta^2(\Delta)} \rangle}{\langle x^2(\Delta) \rangle}. \tag{30}$$

This parameter equals unity for ergodic diffusion processes (indicating the equivalence of the MSD and mean TAMSD).

The non-Gaussianity parameter, $G(\Delta)$, is a sensitive (both theoretical and experimental) indicator used to distinguish the type of a diffusion process observed (e.g., in single-particle tracking experiments [18,111]). In one dimension this parameter is defined as [5,43,47]

$$G(\Delta) = \frac{1}{3} \frac{\langle \overline{\delta^4(\Delta)} \rangle}{\langle \overline{\delta^2(\Delta)} \rangle^2} - 1, \tag{31}$$

where the fourth moment of the time-averaged particle displacement is

$$\overline{\delta^4(\Delta)} = \frac{1}{T-\Delta} \int_0^{T-\Delta} [x(t+\Delta) - x(t)]^4 dt. \tag{32}$$

For Gaussian processes (such as Brownian motion) the non-Gaussianity parameter G is zero, while it can deviate from zero substantially for non-Gaussian processes (e.g., in the diffusing-diffusivity pictures [50], for the dynamics of particles in crowded lipid bilayer membranes [78,104], etc.). We analyze below the behavior of these three higher-order parameters for random-exponent HDPs driven by GCN and experiencing a stratified medium.

B. Distributed scaling exponents: Ergodicity breaking variation with lag time

We here analyze the variation of the ergodicity breaking parameter with the lag time for a stratified, HDP-controlled medium, with a smaller scatter ($\sigma = 0.05$) of the diffusivity-scaling exponent and for an intermediate value of the periodicity, $\delta x = 10$, focusing on the influences of different τ values on $E_{\rm EB}$ for different types of diffusion (negative, zero, and positive values of α_0).

We find that for $\alpha_0 = 0$ the stratified HDP-GCN system reveals the behavior closest to ergodic at short times and the smallest $E_{\rm EB}$ in the whole domain of lag times are realized, followed by $E_{\rm EB}$ for $\alpha_0 = 1$ and $\alpha_0 = -2$ (for $\alpha_0 = -2$ the $E_{\rm EB}$ values are the largest). For all these three choices of the scaling exponent the ratio $E_{\rm EB}/E_0$ is found to decay rapidly for increasing lag times; see the results in Fig. 6. This reflects the respective scatter distributions of individual TAMSD realizations. At very long lag times, supporting the trends of the MSD equivalence to the mean TAMSD at long times in most of the situations, $E_{\rm EB}$ approaches the Brownian limit, so that the ratio $E_{\rm EB}/E_0$ gradually approaches unity for all choices of the scaling exponent α_0. In this limit, the layered HDPs driven by GCN behave effectively as Brownian motion in a homogenized medium (see the long-time limits presented in Figs. 3–5 for confirmation) after the diffusing particles repeatedly cross the barriers between locally heterogeneous layers many times. Generally, we observe that for HDPs driven by GCN in stratified media $E_{\rm EB}$ decays with the lag time faster than E_0 does. At short lag times we observe a scaling of the form $E_{\rm EB}(\Delta) \sim (\Delta/T)^\gamma$ with $\gamma < 1$ such that the ratio $E_{\rm EB}(\Delta)/E_0(\Delta) \sim (\Delta/T)^{\gamma-1}$, apart from the case of larger τ for $\alpha_0 = -2$.

For a fixed $\alpha_0 = 0$ value, when Δ is small the ratio $E_{\rm EB}/E_0$ increases as τ increases. The effect of increasing τ is only weakly pronounced for $\alpha_0 = 1$, and for $\alpha_0 = -2$ the effect of increasing τ is nonsystematic in the regions of short and long lag times, comparing the trends in Fig. 6.

C. Distributed scaling exponents: Nonergodicity variation with lag time

To complement the results for ergodicity breaking, we analyze in Fig. 7 the parameter $E_{\rm NE}$, Eq. (30), as a function of the lag time. We observe that at short lag times for $\alpha_0 = 0$ $E_{\rm NE}$ only moderately increases with increasing correlation time τ, while for $\alpha_0 = 1$ the growth of $E_{\rm NE}$ is much more dramatic (about two orders of magnitude for the range of τ considered), and for $\alpha_0 = -2$ the effect of correlation time is not very systematic. We also find that for $\alpha_0 = 1$ in the region of short lag times Fig. 7 demonstrates that $E_{\rm NE}$ decreases as a power-law function of the lag time Δ. The data of Fig. 7 also shows that in the limit of long times (at $\Delta \gg \tau$) $E_{\rm NE}$ for all choices of the diffusivity scaling exponent becomes nearly insensitive to variation of the correlation time τ and it approaches the value $E_{\rm NE} = 1$ in this limit. This reflects the MSD-mean-TAMSD equality, as already demonstrated in the long-time limits in Figs. 3–5.

D. Distributed scaling exponents: Ergodicity breaking dependence of correlation time τ

Here, we study the effects of variation of the model parameters τ, σ, and δx on $E_{\rm EB}$; see Fig. 8. We find that $E_{\rm EB}$ increases with increasing τ regardless of the diffusion type (the effect is observed for all values of the scaling exponent, for $\alpha_0 = -2$, 0, and 1). For small variance σ the growth of $E_{\rm EB}$ with increasing τ is approximately linear, as indicated in Fig. 8(a). When σ is varied the effects on $E_{\rm EB}$ are not very conclusive, comparing the behaviors in Figs. 8(a) and 8(b). As shown in Fig. 8(c) for $\alpha_0 = -2$, $E_{\rm EB}$ gets progressively

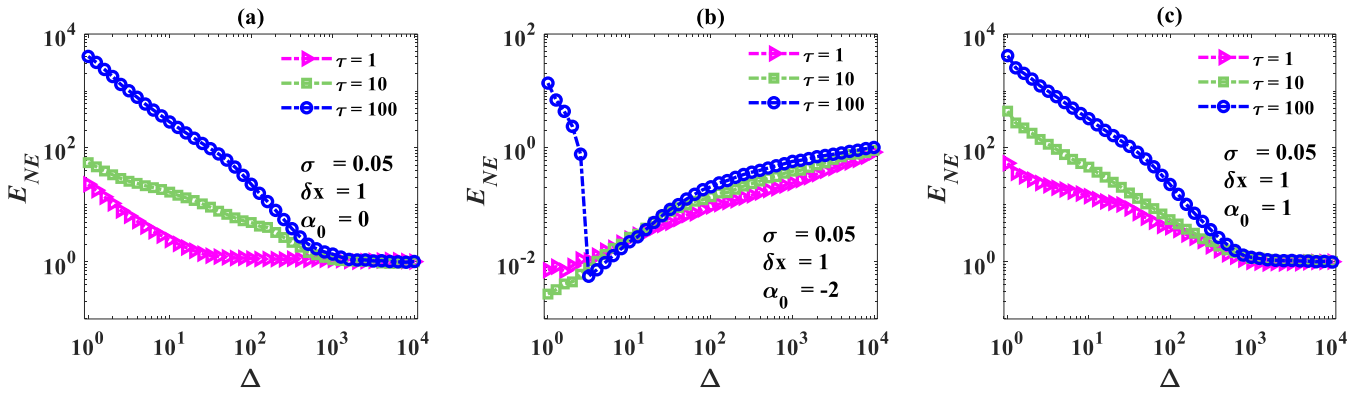

FIG. 7. Complementary ergodicity parameter, $E_{\rm NE}$, as function of the lag time. The green, blue, and pink curves represent HDPs with GCN for $\alpha_0 = 0,\ 1, -2$ (the color scheme is similar to that in Fig. 6). Parameter: $\sigma = 0.05,\ \delta x = 1$, and $\xi_0 = 0$. (a) $\alpha_0 = 0$; (b) $\alpha_0 = -2$; (c) $\alpha_0 = 1$.

smaller for gradually decreasing layer periodicity δx, while the growth of $E_{\rm EB}$ with τ remains roughly linear at small σ [see the indicated slopes in Fig. 8(c)]. The same phenomenon occurs for $\alpha_0 = 0$ and $\alpha_0 = 1$ (not shown). This trend of a more ergodic behavior at smaller periodicity is consistent with the pronounced data overlap and equivalence of the MSD and mean TAMSD for these situations, see Figs. 4(a1), 4(b1), and 4(c1).

E. Distributed scaling exponents: Non-Gaussianity parameter for varying Δ and α_0

We now analyze the behavior of the non-Gaussianity parameter $G(\Delta)$ Eq. (31) in dependence on Δ and α_0. We observe that for small σ values [$\sigma = 0.05$ in Fig. 9(a)] the parameter G at $\alpha_0 = -2$ is larger than that at $\alpha_0 = 1$ and the values of G for the case $\alpha_0 = 0$ are the smallest, indicative of the most Gaussian behavior in this situation (as expected for a homogeneous medium). Moreover, the values of G get smaller as the lag time Δ increases (some G values for $\alpha_0 = 0$ and $\alpha_0 = 1$ are very small and not shown in Fig. 9). For $\alpha_0 = -2$ (both for small and large values of variance σ of the diffusivity exponents) the decrease of $G(\Delta)$ with lag time is found to be roughly $G(\Delta) \sim \Delta^{-1}$, see the scaling shown in Fig. 9. Here, for comparison, we refer the reader to Fig. 5(a) of Ref. [47] with the variation of $G(\Delta)$ for standard HDPs with GWN. When σ becomes comparatively large ($\sigma = 1$), the behavior of $G(\Delta)$ at $\alpha_0 = -2$ almost does not change, as compared to the situation of $\sigma = 0.05$ [comparing Figs. 9(a) and 9(b)]. The largest increase of the non-Gaussianity parameter at larger σ are observed for the case $\alpha_0 = 0$ so that the diffusion becomes progressively non-Gaussian for larger scatters of the scaling exponent of $D(x)$, as intuitively expected.

Finally, in Fig. 10 we present the non-Gaussianity parameter $G(\Delta = 1)$ for varying exponents of $D(x)$ in a wide range. In this figure, the G parameter at the shortest lag time of $\Delta = 1$ is evaluated. We find that for a small spread of scaling exponents [Fig. 10(a)] both for positive and negative values of α the non-Gaussianity parameter attains very large values (strongly non-Gaussian diffusion), while the values of G are small only in the close proximity of $\alpha = 0$, as expected. We refer here to Fig. 5(b) of Ref. [47] where the analysis of $G(\alpha, \Delta = 1)$ dependence was performed for standard HDPs with GWN. We emphasize that $G(\alpha)$ behavior is asymmetric at $\alpha = 0$. As the spreading of the diffusivity exponent increases [see Fig. 10(b)] the values of $G(\alpha)$ increase substantially in the whole range of α, including the case with $\alpha_0 = 0$. We therefore conclude that a considerable spread

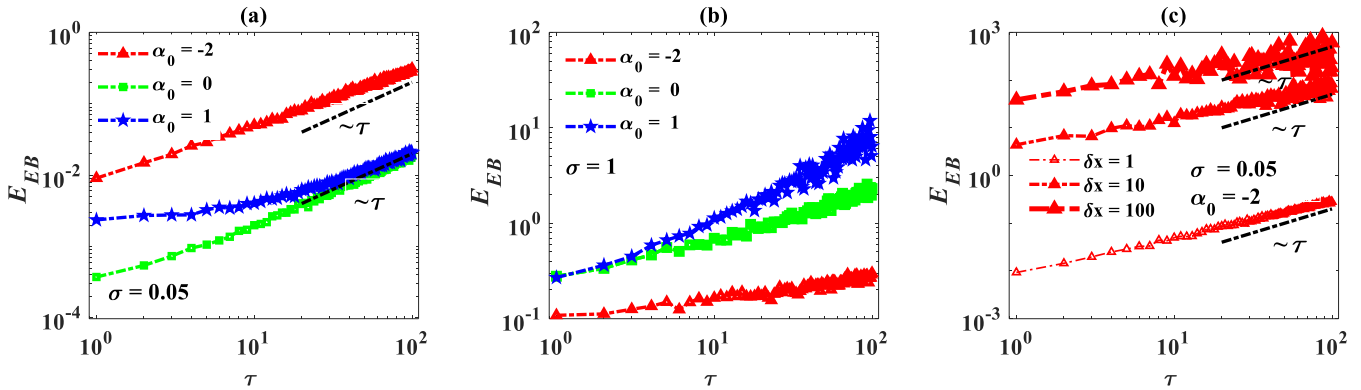

FIG. 8. Variation of $E_{\rm EB}$ as function of the correlation time τ of GCN. The red, green, and blue curves and corresponding symbols indicate the cases $\alpha_0 = -2$, 0, and 1, respectively. Parameters: $\xi_0 = 0$, and (a) $\Delta = 1,\ \delta x = 1,\ \sigma = 0.05$; (b) $\Delta = 1,\ \delta x = 1,\ \sigma = 1$; (c) $\alpha_0 = -2,\ \Delta = 1,\ \sigma = 0.05$. The lines from thin to thick in panel (c) indicate the situations with $\delta x = 1$, 10, and 100, respectively.

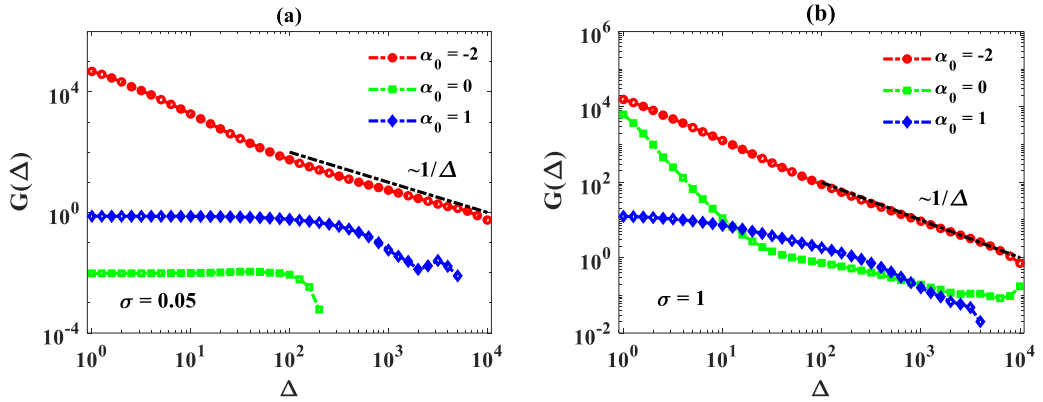

FIG. 9. Variation of the non-Gaussianity parameter $G(\Delta)$ versus lag time Δ, for the values of α_0 given in the legends. Parameters: $\tau = 20$, $\delta x = 10$, $\xi_0 = 0$ and (a) $\sigma = 0.05$ and (b) $\sigma = 1$.

of the scaling exponents of $D(x)$ yields considerably larger values of G, as intuitively expected too.

V. CONCLUSIONS

We have examined the diffusive, nonergodic, and non-Gaussianity characteristics of distributed-exponent HDPs driven by GCN in a stratified medium with quenched disorder. We mainly analyzed the influences from the GCN and diffusion coefficient $D(x)$, namely, the noise correlation time τ, the layer width $2\delta x$ and the variance of the $p(\alpha)$ distribution. The list of the standard statistical classifiers we employed included the MSD, the mean TAMSD, and the distribution of individual TAMSDs. The resulting motion was further quantified in terms of the nonergodicity parameters ($E_{\rm EB}$ and $E_{\rm NE}$) and non-Gaussianity parameter G. In periodic layers of thickness $2\delta x$ the diffusion coefficient has a quenched, random value of the scaling exponent α (following a Gaussian probability density).

For the MSD and TAMSD, we find that the GCN mainly affects the short-time behavior, while it has little influence on the MSD scaling at long times. In detail, the correlation time will induce a pronounced MSD drop at short times, and the initial value of the OU process will impact significantly the scaling exponent. Conversely, the diffusion coefficient $D(x)$ plays the key role in the long-time behavior. The domain length δx can change the diffusion type at long times, e.g., the system changes from normal diffusion to superdiffusion at long times for $\alpha_0 = 1$, and changes to subdiffusion for $\alpha_0 = -2$. Moreover, the fluctuation intensity σ also affects remarkably on the short-time behavior, while it does not change the diffusion type at long times. In fact, when the periodicity of the system is small, the diffusing particle rather rapidly crosses over to vicinal layers. After exploring several layers the diffusion became effectively Brownian. For larger periodicities, the initial motion does not feel the boundary to the next layer, and the resulting motion is more nonergodic. This nonergodicity is the inherent property of anomalous diffusion in a medium with space-dependent diffusivity [40,47].

Layered HDPs reflect quenched heterogeneous systems consisting of periodic layers, in which each layer itself is characterized by a position-varying diffusivity. Depending on the exact value of the associated local scaling exponent the resulting effective drift directs the particles preferentially to the layer center or to the boundaries to the vicinal layers. This could correspond to the motion of biopolymers or tracers in layers of cells, for instance, in some biological tissues, in which each cell has somewhat different densities

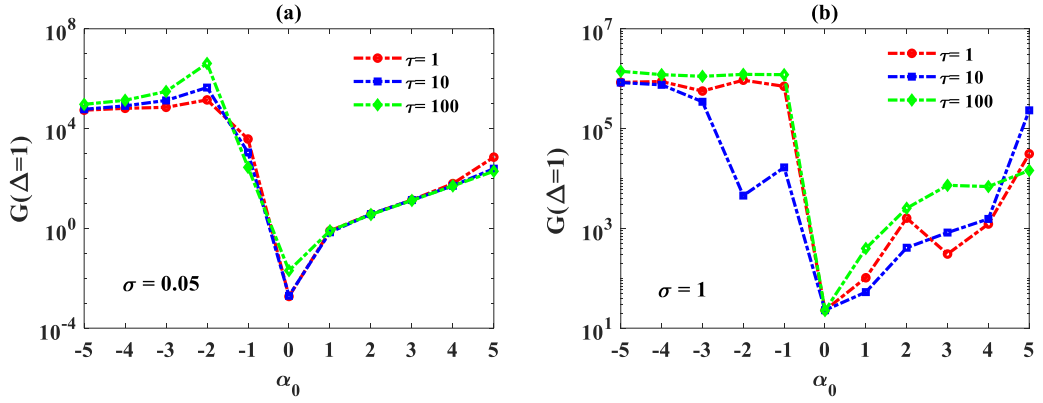

FIG. 10. Non-Gaussianity parameter as function of α_0, plotted for noise correlation times $\tau = 1$, 10, and 100 (respectively, the red, blue, and green symbols). Parameters: medium periodicity $\delta x = 10$, lag time $\Delta = 1$, $\xi_0 = 0$ and for panels (a) and (b) the variance of $p(\alpha)$ distribution is $\sigma = 0.05$ and 1, correspondingly. A Gaussian distribution, for comparison, has $G = 0$ for all Δ.

of macromolecules acting as obstacles of tracer motion, and additionally each cell is inhomogeneous by itself. Similar situations may occur in artificial systems such as liquid crystalline layers or layered structures in groundwater aquifers. We note that thermophoresis of Brownian particles driven by colored noise was studied in Ref. [111]. It was demonstrated that as a response to temperature gradients the particles can accumulate in colder (positive thermophoresis) or hotter (negative thermophoresis) regions depending on their temperature-varying mobility. Further studies of spatial correlations, diffusivity forms different from power-law functions of position x, or slowly time-varying α-values or medium periodicities $2\delta x$ will be of interest. Understanding the differences between the overdamped and underdamped limits of this and related problems would also be interesting to rationalise in the future. Finally, our results may provide new mathematical understanding of heterogeneous diffusion and nonergodicity observed in various physical systems in the presence of quenched disorder, especially when the asymptotic behavior has not yet been reached.

ACKNOWLEDGMENTS

This work was supported by the NSF of China (Grants No. 11772255 No. 11902118), the National Key Research and Development Program of China under Grant No. 2018AAA0102201, the Research Funds for Interdisciplinary Subject of Northwestern Polytechnical University, the Shaanxi Project for Distinguished Young Scholars, the Shaanxi Provincial Key R&D Program 2020KW-013 and 2019TD-010. RM acknowledges financial support by the Deutsche Forschungsgemeinschaft (DFG Grant No. ME 1535/7-1). RM also thanks the Foundation for Polish Science (Fundacja na rzecz Nauki Polskiej) within an Alexander von Humboldt Polish Honorary Research Scholarship.

APPENDIX

From Eq. (27), we derive the MSD for a stratified medium. The only parameter to be determined is the escape rate λ. Generally, λ can be given by the inverse of the mean first exit time T that a particle starts from the middle of a layer and reaches either middle point of its adjacent layers. For a particle within the interval $(-2\delta x,\ 2\delta x)$ starting from point x, we denote the mean first exit time as $T(x)$.

When $|\alpha|$ is small, it means $D(x) = D_0(|x|^\alpha + D_{\rm off})$ does not vary quickly in the domain of $(-2\delta x,\ 2\delta x)$. Then $T(x)$ can be well approximated by the Pontryagin equation [112], which takes the form

$$D(x)\frac{\partial^2}{\partial x^2}T(x) = -1, \qquad T(-2\delta x) = T(2\delta x) = 0, \tag{A1}$$

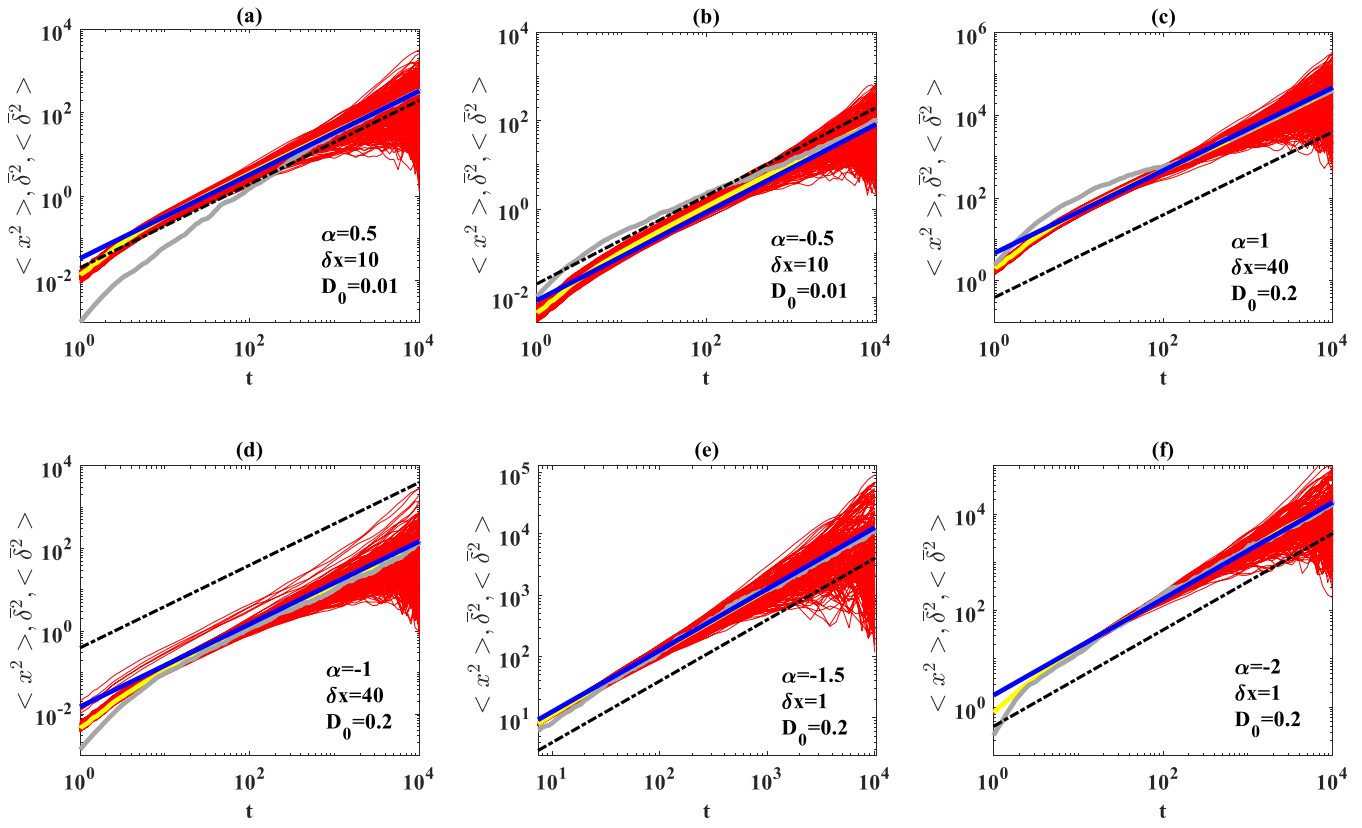

FIG. 11. When $|\alpha| \leqslant 1$ in panels (a)–(d), the blue line is the theoretical result given above. The theoretical results fit well with numerical simulations for large δx. When $|\alpha| > 1$ in panels (e) and (f), λ is obtained by numerically calculating the mean first exit time from the Langevin equation. The blue line is $\langle x^2(t)\rangle = 4\lambda\delta x^2 t$, which fits well with numerical simulation for small δx. The initial position is $x_0 = 0.1$, the gray line is the MSD and yellow line is the mean TAMSD.

and $\lambda = 1/T(0)$. When $\alpha = 1$, Eq. (A1) can be solved and the escape rate takes $\lambda = D_0/(2\delta x[\ln(2\delta x) - 1])$ omitting the small number $D_{\rm off}$. Consequently, we get the approximate MSD as

$$\langle x^2(t)\rangle = 2\frac{D_0\delta x}{\ln(2\delta x) - 1}t. \tag{A2}$$

We find that when δx is large, the approximation fits well with the numerical result for the long-time behavior [see Fig. 4(b3) and Figs. 11(c) and 11(d)], while a small δx value leads to discrepancies. For example, when $\delta x = 1$, λ is negative such that the approximation Eq. (A2) is invalid. Similarly, we can get the MSD for small $|\alpha|$, such as $\alpha = 0.2$ for $\langle x^2(t)\rangle = \frac{144D_0\delta x^2}{25(2\delta x)^{0.8}}t$; $\alpha = 0.5$ for $\langle x^2(t)\rangle = \frac{3D_0\sqrt{\delta x}}{2\sqrt{2}}t$; $\alpha = -0.5$ for $\langle x^2(t)\rangle = \frac{15D_0}{4\sqrt{2\delta x}}t$. The corresponding theoretical results and numerical simulations are presented in Fig. 11, and show a good match.

When $|\alpha|$ is large, $D(x) = D_0(|x|^\alpha + D_{\rm off})$ varies quickly in the domain of $(-2\delta x,\ 2\delta x)$. It is no longer appropriate to use the Pontryagin equation. Moreover, when δx is large, the diffusivity in a layer has huge maximum and minimum values. Especially, when $\alpha = -2$, $D(x)$ is so small for large $|x|$ that it is difficult for a particle to cover a large distance and jump to another layer. Consequently, it will even fail to take the heterogeneous diffusion as a random walk at any finite time. However, when δx is small, the method still works. To examine the validity, we numerically get the mean first exit time of a particle starting from x_0 where $D(x)$ has the minimal value, and exiting either $x_0 + 2\delta x$ or $x_0 - 2\delta x$. Then with $\langle x^2(t)\rangle = 4\lambda\delta x^2$, we can still get a good result, see Figs. 11(e) and 11(f).

[1] J. P. Bouchaud and A. Georges, Phys. Rep. **195**, 127 (1990).
[2] R. Metzler and J. Klafter, Phys. Rep. **339**, 1 (2000); J. Phys. A **37**, R161 (2004).
[3] R. Metzler, J. H. Jeon, A. G. Cherstvy, and E. Barkai, Phys. Chem. Chem. Phys. **16**, 24128 (2014).
[4] S. Havlin and D. Ben-Avraham, Adv. Phys. **51**, 187 (2002).
[5] F. Höfling and T. Franosch, Rep. Prog. Phys. **76**, 046602 (2013).
[6] S. Burov, J.H. Jeon, R. Metzler, and E. Barkai, Phys. Chem. Chem. Phys. **13**, 1800 (2011).
[7] I. M. Sokolov, Soft Matter **8**, 9043 (2012).
[8] Y. Meroz and I. M. Sokolov, Phys. Rep. **573**, 1 (2015).
[9] R. Metzler, J.H. Jeon, and A. G. Cherstvy, Biochem. Biophys. Acta BBA-Biomembr. **1858**, 2451 (2016).
[10] Y. He, S. Burov, R. Metzler, and E. Barkai, Phys. Rev. Lett. **101**, 058101 (2008).
[11] J.H. Jeon, V. Tejedor, S. Burov, E. Barkai, C. Selhuber-Unkel, K. Berg-Sorensen, L. Oddershede, and R. Metzler, Phys. Rev. Lett. **106**, 048103 (2011).
[12] H. Zuo, Z. Gu, H. Cooper, and Z. Xu, J. Colloid Interf. Sci. **459**, 10 (2005); Z. Gu, H. Zuo, L. Li, A. Wu, and Z. Xu, J. Mater. Chem. B **3**, 3331 (2015).
[13] X. Liang, H. Wang, Y. Zhu, R. Zhang, V. Cogger, X. Lin, Z. Xu, J. Grice, and M. Roberts, ACS Nano **10**, 387 (2016).
[14] K. Nørregaard, R. Metzler, C. M. Ritter, K. Berg-Sørensen, and L. B. Oddershede, Chem. Rev. **117**, 4342 (2017).
[15] B. Lin and J. Goree, Phys. Rev. Lett. **100**, 055003 (2008).
[16] J. Mattsson, H. Wyss, A. Nieves, K. Miyazaki, Z. Hu, D. Reichman, and D. Weitz, Nature **462**, 83 (2009).
[17] E. Weeks and D. Weitz, Chem. Phys. **284**, 361 (2002).
[18] C. Manzo and M. Garcia-Parajo, Rep. Prog. Phys. **78**, 124601 (2015).
[19] I. Golding and E. Cox, Phys. Rev. Lett. **96**, 098102 (2006).
[20] J. Szymanski and M. Weiss, Phys. Rev. Lett. **103**, 038102 (2009).
[21] J.H. Jeon, N. Leijnse, L. Oddershede, and R. Metzler, New J. Phys. **15**, 045011 (2013).
[22] T. Kuhn, T. Ihalainen, J. Hyvaluoma, N. Dross, S. Willman, J. Langowski, M. Vihinen-Ranta, and J. Timoen, PLoS One **6**, e22962 (2011).
[23] K. Kruse and A. Iomin, New. J. Phys. **10**, 023019 (2008).
[24] C. Nicholson, Rep. Prog. Phys. **64**, 815 (2001).
[25] E. Barkai, Y. Garini, and R Metzler, Phys. Today **65**, 29 (2012).
[26] D. Krapf and R. Metzler, Phys. Today **72**, 48 (2019).
[27] F. Amblard, A. Maggs, B. Yurke, A. Pargellis, and S. Leibler, Phys. Rev. Lett. **77**, 4470 (1996).
[28] M. Geza and J. McCray, J. Env. Manag. **88**, 393 (2008).
[29] H. Scher, G. Margolin, R. Metzler, J. Klafter, and B. Berkowitz, Geophys. Res. Lett. **29**, 5-1 (2002).
[30] R. Schumer, D. A. Benson, M. M. Meerschaert, and B. Baeumer, Water Resour. Res. **39**, 1296 (2003).
[31] E. Bunde, A. Bunde, S. Havlin, and H. Roman, Phys. Rev. Lett. **81**, 729 (1998).
[32] E. Chai and C. Lim, J. Phys. A **45**, 145001 (2012).
[33] S. Havlin, Phys. Rev. B **34**, 445 (1986).
[34] P. Siegle, I. Goychuk, and P. Hänggi, Phys. Rev. Lett. **105**, 100602 (2010).
[35] M. Dentz, P. Gouze, A. Russian, J. Dweik, and F. Delay, Adv. Water Resour. **49**, 13 (2012).
[36] R. Maxwell, L. Condon, S. Kollet, K. Maher, R. Haggerty, and M. Forrester, Geophys. Res. Lett. **43**, 701 (2016).
[37] B. English, V. Hauryliuk, A. Sanamrada, S. Tankov, N. Dekker, and J. Elf, Proc. Natl. Acad. Sci. USA **108**, E365 (2011).
[38] I. Wong, M. Gardel, D. Reichman, E. Weeks, M. Valentine, A. Bausch, and D. Weitz, Phys. Rev. Lett. **92**, 178101 (2004).
[39] C. Lee, A. Crosby, T. Emrick, and R. Hayward, Macromol. **47**, 741 (2014).
[40] A. G. Cherstvy, A. V. Chechkin, and R. Metzler, New J. Phys. **15**, 083039 (2013); J. Phys. A **47**, 485002 (2014).
[41] A. G. Cherstvy, and R. Metzler, Phys. Chem. Chem. Phys. **15**, 20220 (2013); J. Stat. Mech. (2015) P05010.
[42] A. G. Cherstvy, A. V. Chechkin, and R. Metzler, Soft Matter **10**, 1591 (2014).
[43] S. K. Ghosh, A. G. Cherstvy, D. S. Grebenkov, and R. Metzler, New J. Phys. **18**, 013027 (2016).
[44] A. Fulinski, J. Chem. Phys. **138**, 021101 (2013).
[45] J. Spiechowicz, J. Łuczka, and P. Hänggi, Sci. Rep. **6**, 30948 (2016).

[46] W. Guo, Y. Li, W. Song, and L. Du, J. Stat. Mech. (2018) 033303.

[47] A. G. Cherstvy and R. Metzler, Phys. Rev. E **90**, 012134 (2014); J. Chem. Phys. **142**, 144105 (2015).

[48] V. Sposini, A. V. Chechkin, F. Seno, G. Pagnini, and R. Metzler, New J. Phys. **20**, 043044 (2018).

[49] Y. Sato and R. Klages, Phys. Rev. Lett. **122**, 174101 (2019).

[50] A. V. Chechkin, F. Seno, R. Metzler, and I. M. Sokolov, Phys. Rev. X **7**, 021002 (2017).

[51] D. Grebenkov, R. Metzler, and G. Oshanin, Comm. Chem. **1**, 96 (2018).

[52] Y. Lanoiselee and D. S. Grebenkov, J. Phys. A **51**, 145602 (2018); Y. Lanoiselee, N. Moutal, and D. S. Grebenkov, Nat. Commun. **9**, 4398 (2018).

[53] J. Slezak, K. Burnecki, and R. Metzler, New J. Phys. **21**, 073056 (2019).

[54] Z. Budrikis, Solid State Phys. **65**, 109 (2014).

[55] S. Haravifard, Z. Yamani, and B. Gaulin, *Experimental Methods in the Physical Sciences* (Academic Press, San Diego, CA, 2015).

[56] K. P. Ramesh, Annu. Rep. NMR Spectr. **71**, 139 (2010).

[57] F. Kun, Creep Fatigue Pol. Matrix Comp. 327 (2011).

[58] H. Scher and E. W. Montroll, Phys. Rev. B **12**, 2455 (1975).

[59] E. M. Bertin and J. P. Bouchaud, Phys. Rev. E **67**, 026128 (2003).

[60] S. Burov and E. Barkai, Phys. Rev. Lett. **98**, 250601 (2007).

[61] H. Krüsemann, R. Schwarzl, and R. Metzler, Transp. Porous Media **115**, 327 (2016).

[62] R. Valiullin, Ann. Rep. NMR Spectr. **79**, 23 (2013).

[63] Y. Li, Y. Xu, and J. Kurths, Phys. Rev. E **96**, 052121 (2017).

[64] Y. Li, Y. Xu, J. Kurths, and X. Yue, Chaos **27**, 103102 (2017); Y. Li, Y. Xu, and J. Kurths, Phys. Rev. E **99**, 052203 (2019).

[65] J. Feng, W. Xu, Y. Xu, and X. Wang, J. Phys. A **531**, 121747 (2019).

[66] Y. Xu, W. Zan, W. Jia, and J. Kurths, J. Comp. Phys. **394**, 41 (2019).

[67] Y. Xu, H. Li, H. Wang, W. Jia, X. Yue, and J. Kurths, J. Appl. Mech. **84**, 091004 (2017).

[68] R Mei, Y Xu, and J Kurths, Phys. Rev. E **100**, 022114 (2019).

[69] J. Ma, Y. Xu, J. Kurths, H. Wang, and W. Xu, Chaos. **28**, 113601 (2018).

[70] J. H. Jeon, E. Barkai, and R. Metzler, J. Chem. Phys. **139**, 121916 (2013).

[71] H. Yang, G. Luo, P. Karnchanaphanurach, T-M. Louie, I. Rech, S. Cova, L. Xun, and X. S. Xie, Science **302**, 262 (2003).

[72] S. C. Kou and X. Xie, Phys. Rev. Lett. **93**, 180603 (2004).

[73] X. Hu, L. Hong, M. D. Smith, T. Neusius, X. Cheng, and J. C. Smith, Nat. Phys. **12**, 171 (2016).

[74] A. M. van Oijen, P. C. Blainey, D. J. Crampton, C. C. Richardson, T. Ellenberger, and X. S. Xie, Science **301**, 1235 (2003).

[75] W. Deng and E. Barkai, Phys. Rev. E **79**, 011112 (2009).

[76] M. Schwarzl, A. Godec, and R. Metzler, Sci. Rep. **7**, 3878 (2017).

[77] T. Albers and G. Radons, Phys. Rev. Lett. **120**, 104501 (2018).

[78] M. Song, H. Moon, J.H. Jeon, and H. Park, Nat. Comm. **9**, 344 (2018).

[79] P. Hänggi and P. Jung, Adv. Chem. Phys. **89**, 239 (1995).

[80] H. Li, Y. Xu, J. Kurths, and X. Yue, Eur. Phys. J. B **92**, 76 (2019); H. Li, Y. Xu, X. Yue, and J. Kurths, J. Phys. A 121764 (2019).

[81] Q. Liu, Y. Xu, C. Xu, and J. Kurths, Appl. Math. Model. **64**, 249 (2018).

[82] D. Liu, Y. Xu, and J. Li, Chaos, Solitons Fract. **104**, 806 (2017).

[83] Y. Xu, R. Mei, Y. Li, and J. Kurths, Springer Proc. Math. Stat. **282**, 443 (2019); Y. Li, Y. Xu, W. Xu, Z. Deng, and J. Kurths, Phys. Rev. E **96**, 022152 (2017); Y. Li, R. Mei, Y. Xu, J. Kurths, J. Duan, and R. Metzler, New J. Phys. **22**, 053016 (2020).

[84] M Polettini, J. Stat. Mech. (2013) P07005.

[85] V. Blickle, T. Speck, C. Lutz, U. Seifert, and C. Bechinger, Phys. Rev. Lett. **98**, 210601 (2007).

[86] A. Lau and T. Lubensky, Phys. Rev. E **76**, 011123 (2007).

[87] P. Hänggi, Helv. Phys. Acta. **51**, 183 (1978).

[88] N. Leibovich and E. Barkai, Phys. Rev. E **99**, 042138 (2019).

[89] M. Heidernätsch, *On the Diffusion in Inhomogeneous Systems*, Ph.D. Thesis, University of Chemnitz (2015).

[90] K. Itô, Memoirs Amer. Math. Soc. **4**, 51 (1951).

[91] L. Fisk, Trans. Amer. Math. Soc. **120**, 369 (1965).

[92] L. Stratonovich, J. SIAM Control **4**, 362 (1966).

[93] L. Klimontovich, Physica A **163**, 515 (1990).

[94] M. Sokolov, Chem. Phys. **375**, 359 (2010).

[95] R. Mannella and E. McClintock, Fluct. Noise Lett. **11**, 1240010 (2012).

[96] G. Volpe and J. Wehr, Rep. Prog. Phys. **79**, 053901 (2016).; R. Honeycutt, Phys. Rev. A **45**, 604 (1992).

[97] K. Mallick and P. Marcq, J. Phys. A **37**, 4769 (2004).

[98] H. G. Duan and X. T. Liang, Eur. Phys. J. B **85**, 209 (2012).

[99] J. P. Bouchaud, J. Phys. I France **2**, 1705 (1992).

[100] R. Hou, A. G. Cherstvy, R. Metzler, and T. Akimoto, Phys. Chem. Chem. Phys. **20**, 20827 (2018).

[101] J. H. P. Schulz, E. Barkai, and R. Metzler, Phys. Rev. Lett. **110**, 020602 (2013); Phys. Rev. X **4**, 011028 (2014).

[102] G. E. Uhlenbeck and L. S. Ornstein, Phys. Rev. **36**, 823 (1930).

[103] J. H. Jeon, M. Javanainen, H. Martinez-Seara, R. Metzler, and I. Vattulainen, Phys. Rev. X **6**, 021006 (2016).

[104] X. Brokmann, J. P. Hermier, G. Messin, P. Desbiolles, J. P. Bouchaud, and M. Dahan, Phys. Rev. Lett. **90**, 120601 (2003).

[105] G. Margolin and E. Barkai, Phys. Rev. Lett. **94**, 080601 (2005).

[106] S. Thapa, A. G. Cherstvy, N. Lukat, C. Selhuber-Unkel, and R. Metzler, J. Chem. Phys. **150**, 144901 (2019).

[107] A. Andereanov and D. S. Grebenkov, J. Stat. Mech. (2012) P07001.

[108] A. G. Cherstvy, S. Thapa, Y. Mardoukhi, A. V. Chechkin, and R. Metzler, Phys. Rev. E **98**, 022134 (2018).

[109] A. Godec and R. Metzler, Phys. Rev. Lett. **110**, 020603 (2013).

[110] D. Ernst, J. Koehler, and M. Weiss, Phys. Chem. Chem. Phys. **16**, 7686 (2014).

[111] S. Hottovy, G. Volpe, and J. Wehr, Europhys. Lett. **99**, 60002 (2012).

[112] L. Pontryagin, A. Andronov, and A. Witt, Zh. Eksp. Teor. Fiz. **3**, 172 (1933); reprinted in *Noise in Nonlinear Dynamical Systems*, edited by F. Moss and P. V. E. McClintock (Cambridge University Press, Cambridge, UK, 1989), Vol. 1, p. 329.